Journal of Volcanology and Geothermal Research 341 (2017) 269–286

Contents lists available at ScienceDirect

Journal of Volcanology and Geothermal Research

journal homepage: www.elsevier.com/locate/jvolgeores

Fluid-driven uplift at Long Valley Caldera, California: Geologic perspectives

Wes Hildreth

Volcano Science Center, U.S. Geological Survey, Menlo Park, California, United States

ARTICLE INFO

Article history:
Received 17 January 2017
Received in revised form 3 May 2017
Accepted 12 June 2017
Available online 15 June 2017

ABSTRACT

Since persistent seismicity began in the Sierra Nevada adjacent to Long Valley caldera in 1978–1980, intracaldera unrest has been marked by (1) episodes of uplift totaling ~83 cm, centered on the middle Pleistocene resurgent dome, and (2) recurrent earthquake swarms along a 12-km-long segment of the caldera's ring-fault zone that is contiguous with both the dome and the Sierran seismogenic domain. Others have attributed the recent unrest to magmatic intrusion(s), but it is argued here that evidence for new magma is lacking and that ongoing uplift and ring-fault-zone seismicity are both promoted by ascent of aqueous fluid released by second boiling of the residue of the enormous Pleistocene rhyolitic reservoir terminally crystallizing at depths ≥10 km. For 2 Myr, eruptive vent clusters migrated southwestward from Glass Mountain to Mammoth Mountain. There has been no eruption on the resurgent dome since 500 ka, and since 230 ka volcanism has been restricted to the caldera's west moat and contiguous Sierran terrain, both outside the structural caldera. High-temperature hydrothermal activity in the central caldera waned after ~300 ka, cooling the Pleistocene rhyolitic focus to the extent that drilling on the resurgent dome found mid-caldera temperature to be only 100 °C and isothermal at depths of 2–3 km. Beneath most of the resurgent dome, there is little seismicity at any depth, no emission of magmatic CO_2 or other magmatic gases, no elevated $^3He/^4He$ ratios, and only normal to below-normal heat flow. Most of the 75-km-long ring-fault zone is likewise aseismic, excepting only the 12-km segment contiguous with the extracaldera seismogenic domain in the Sierra. Since 1980, the Sierran seismicity has released 3.6 times more cumulative seismic energy than have intracaldera earthquakes. The caldera seismicity is not driven by stresses associated with the adjacent uplift but, instead, by the extracaldera tectonic stressfield. Sierran seismicity activated the directly contiguous south-moat segment of the ring-fault zone, which had originated in the caldera-forming eruption at 767 ka and everywhere else remains sealed. Hypocenter relocation studies of 1000s of earthquakes along the seismic segment have resolved recurrent upward-migrating swarms within networks of cryptic faults, apparently triggered by rapidly ascending pulses of high-pressure low-viscosity aqueous fluid. Entering the brittle crust at depths of 8–10 km, such fluid is just what should be expected from second boiling of the late-stage CO_2-poor rhyolitic residue. The fluid provides the pressure source above the apex of the crystallizing caldera-wide pluton and then escapes laterally to the newly reactivated southern segment of the ring-fault zone, its only available permeable pathway, where it mediates the ongoing south-moat seismicity.

Published by Elsevier B.V.

1. Introduction

Review and reconsideration of all geological and geophysical data led Hildreth (2004) to conclude that the Long Valley rhyolitic magma chamber, so active in the middle Pleistocene, is now moribund. Numerous tomographic attempts to identify a magma body beneath the caldera failed to image one convincingly, and few further attempts were made after 1998 when the LVEW corehole found the center of the resurgent dome (Figs. 1, 2) to be isothermal at 100 °C at depths of 2 to 3 km.

Uplift of the Pleistocene resurgent area by ~83 cm, in several pulses since 1980, however, has been modeled by some as magmatic intrusion of a prolate spheroid, a textbook model, at a depth of ~7 km (Langbein, 2003; Montgomery-Brown et al., 2015). Any discussion of the ongoing uplift, however, needs to make clear the model's conceptual relation to (or distinction from) that of the extensive subcaldera magma chamber envisioned by most investigators prior to 1998 but long since widely considered a dead horse.

Cumulative uplift of ~83 cm since 1980 has been centered directly beneath the Pleistocene resurgent structure, which had been updomed 400–500 m by early postcaldera resurgence (most of that uplift having been over by 570 ka; Hildreth et al., 2017). The ongoing uplift has been punctuated by short pulses of more rapid rise in 1980, 1982, 1983, 1989–90, and 1997–98, as summarized and illustrated by Hill et al. (2002) and Hill (2006), plus a resumption of 3–5 cm of additional uplift since 2011 (Montgomery-Brown et al., 2015).

Is the current uplift thought to be promoted by reactivation of residual magma of the formerly great Long Valley intracrustal chamber, by

E-mail address: hildreth@usgs.gov.

http://dx.doi.org/10.1016/j.jvolgeores.2017.06.010
0377-0273/Published by Elsevier B.V.

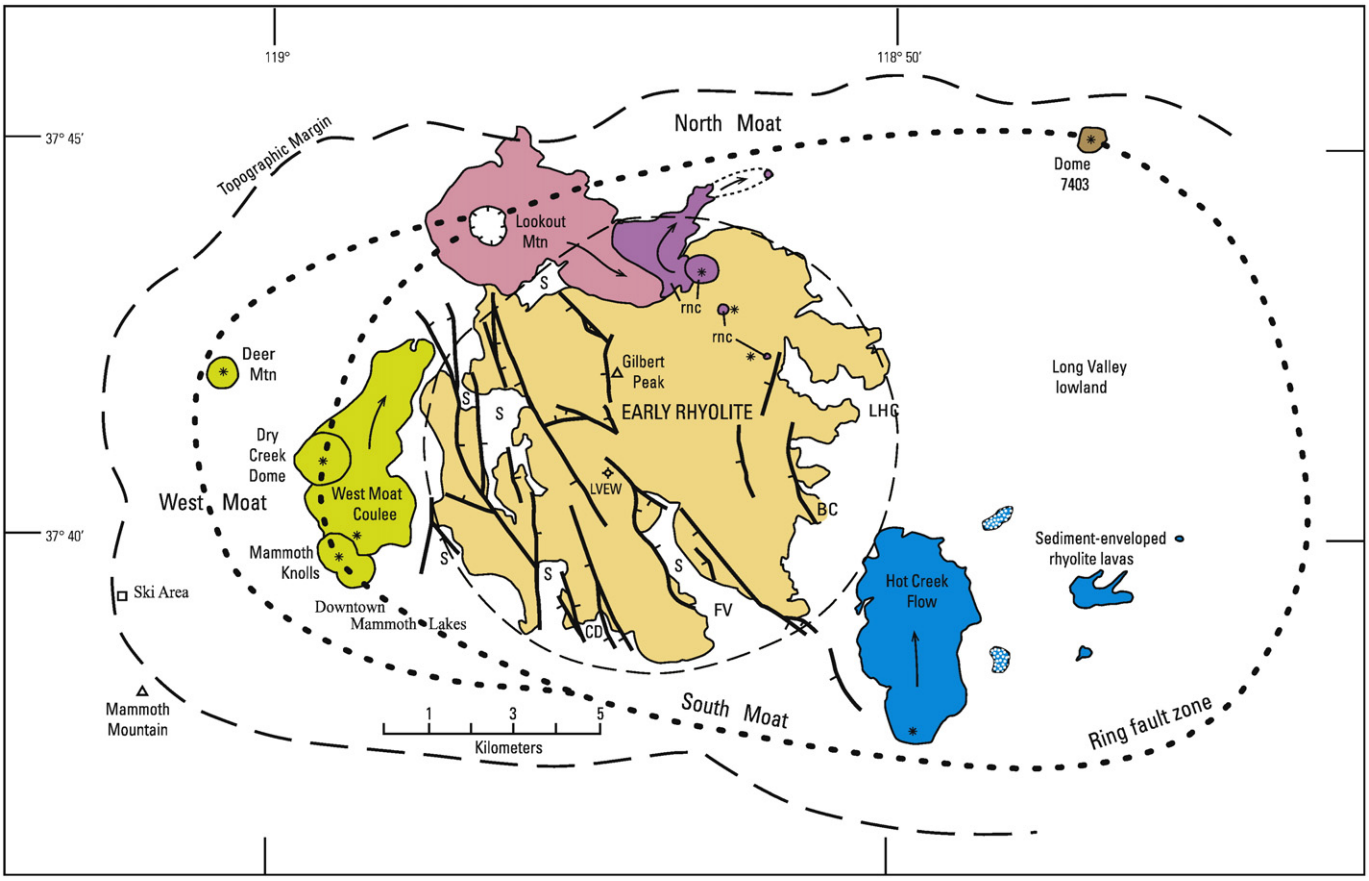

Fig. 1. Long Valley postcaldera rhyolites. Early Rhyolite (750–640 ka) in orange is cut by numerous faults associated with structural resurgent uplift, which is outlined in long dashes. Lookout Mountain in red is also Early Rhyolite (~680 ka) but is not deformed. Three sets of Moat Rhyolite lavas crop out in north (unit **rnc**; 570–505 ka, purple), southeast (362–328 ka, blue), and west (150–100 ka, green). The north and west sets are all crystal-rich, as are the two patterned lavas in the southeast set. Four (of the six) units in the southeast set and all of the Early Rhyolites are phenocryst-poor (0–3 wt% crystals). Dome 7403 in the northeast moat, uniquely rhyodacitic, is undated. Arrows generalize lava flow directions. 680-ka lava from Lookout Mountain flowed onto later area of resurgent uplift; 570-ka lava **rnc** flowed from its vent on the uplift steeply down into the north moat, subsequent to most of the resurgent uplift. Estimated position of main ring-fault zone is 2–4 km inboard of topographic margin, which receded by syncollapse landsliding and by subsequent erosion; see also Fig. 3. Complexly stepped structure of concealed faults in west moat, inferred from drillholes (Hildreth, 2017), is enclosed by pair of dotted lines. Abbreviations: BC, Blue Chert; CD, Casa Diablo geothermal plant; FV, Fumarole Valley; LHC, Little Hot Creek; LVEW, Long Valley Exploratory Well, 3 km deep, high on resurgent uplift; S, surficial deposits filling structural lows on resurgent uplift, notably Fumarole Valley graben to the southeast and Smokey Bear Flat graben to the west.

ascent of a new intrusion from greater depth, or by pressurization of aqueous fluid? Is the prolate pressure-source model envisaged to consist of melt, of mobile crystal mush with interstitial melt, of buoyant ductile solid, or of expanding aqueous vapor in a fracture network? Is it more likely that present-day uplift be related to expulsion of fluid from the crystallizing residue of the former rhyolitic chamber by "second boiling," to bulk remobilization of that residue, or to an independent brand-new intrusion?

The author has restudied the geologic and eruptive history of Long Valley caldera and its periphery in greater detail than previous work, remapping the area at 1:24,000 scale, and (with USGS colleagues, Andrew Calvert and Judy Fierstein) has radioisotopically dated nearly all eruptive units (Hildreth et al., 2014, 2017; Hildreth and Fierstein, 2016a, 2016b). There has never been a *non*-rhyolitic eruption inside the structural caldera, which formed by collapse 767,000 years ago, and the most recent rhyolitic eruptions were ~330 ka in the caldera's southeast moat and ~100 ka in the west moat (Figs. 1, 2). There has been no eruption on the caldera's resurgent dome in 500,000 years. Numerous mafic eruptions peripheral to Mammoth Mountain (and parental to that 100–50 ka dacite edifice itself) began ~230 ka, issuing from vents outside the caldera's structural margin and compositionally unrelated to the Long Valley rhyolitic system.

Fig. 2 summarizes the southwestward migration of eruptive foci for the last 2 Myr. Vents for the successive episodes are clustered, not scattered randomly. It would be unprecedented for a new intrusion today to backtrack to the mid-caldera beneath the resurgent dome. Mantle-derived mafic magma (basalt or trachyandesite) has not erupted on the site of the caldera for >2.5 Myr. The domain of mantle productivity that energized crustal melting and rhyolitic magmatism for nearly 2 Myr withdrew southwestward from Long Valley a quarter-million years ago.

The geochronologically calibrated geological and volcanological history and the weakness of CO_2 emission, seismicity, and thermal signal beneath the major part of the caldera and its Pleistocene resurgent dome make me deeply skeptical that the recent uplift is caused by a new magmatic intrusion. The following discussions present the basis of my doubts and my perplexity about related geophysical overinterpretations.

Rather than a new magmatic injection, evidence and inferences are developed here that the pressure source for ongoing uplift is low-viscosity aqueous fluid ascending from the remainder of the once voluminous, now moribund, rhyolitic magma chamber—as its residue finally crystallizes completely to granite and expels its residual volatiles by "second boiling."

2. Isobaric "second boiling"

Exsolution of a $CO_2 + H_2O$ vapor phase by nucleation and growth of gas bubbles in a fluid-saturated granitic (rhyolitic) magma, induced by decompression during magma ascent or roof-rock failure, has

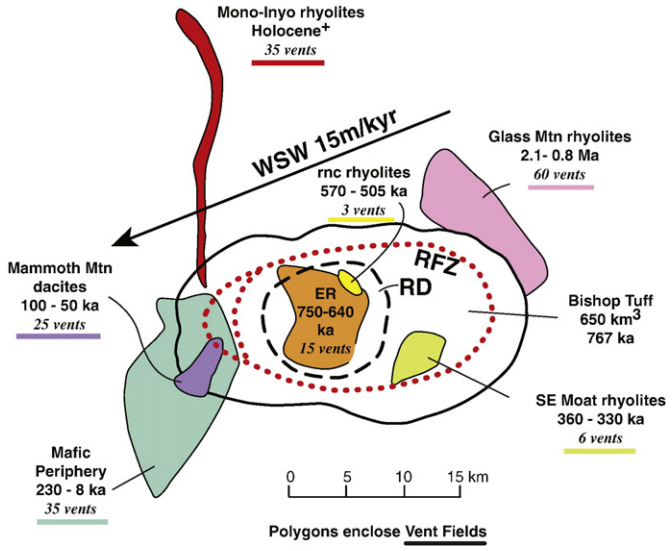

Fig. 2. Migration of vent clusters for main sets of eruptions in Long Valley area, from 2 Ma to Holocene. Magma chamber from which Bishop Tuff erupted during caldera collapse at 767 ka is outlined by ring-fault zone (dotted, RFZ). Dashed line indicates Pleistocene resurgent dome (RD), on the site of which a vent cluster released ~100 km^3 of Early Rhyolite (ER), mostly prior to the structural resurgent uplift. Mammoth Mountain dacite edifice is surrounded by basaltic volcanic field (Fig. 5), which thermally sustained some crystal-rich Long Valley rhyolite beneath the caldera's west moat (Fig. 1). Mono-Inyo rhyolites, dominantly postglacial but as old as 41 ka, erupted along rangefront fault zone from a discrete magmatic system focussed under Mono Craters.

sometimes been called "first boiling" (Candela, 1997). After such a felsic magma body ceases ascent and has been emplaced in the upper crust (at a depth influenced by neutral buoyancy and/or roof-rock strength), progressive crystallization may successively produce increasingly crystal-rich but still-mobile magma, sluggish crystal mush, locked-up (rigid) crystal sponge, and finally a solid rind—ideally in concentric shells against the roof and upper walls. Advanced crystallization of anhydrous phases (feldspars and quartz) decreases the residual melt fraction, increases its vapor pressure, and promotes gas exsolution within the crystal mush and in the increasingly rigid outer-upper shell of the stagnant pluton. Isobaric gas exsolution compelled by advancing crystallization in such late-stage granitic magma has been called "second boiling."

At the shallow upper-crustal levels inferred for the caldera-forming Bishop Tuff rhyolite (150–300 MPa; Wallace et al., 1999; Scaillet and Hildreth, 2001; Roberge et al., 2013; Evans et al., 2016; ~6–12 km depths), most CO_2 would have earlier exsolved from the rhyolitic melt owing to its low solubility, rendering the residual volatile phase to be nearly pure water. Water saturation in rhyolitic melt is attained at ~4 wt% H_2O at 100 MPa, ~6 wt% at 200 MPa, and ~8 wt% at 300 MPa (Tuttle and Bowen, 1958). Melt inclusions trapped in quartz phenocrysts in the 650-km^3 Bishop Tuff contain 4–6 wt% H_2O (Wallace et al., 1999), and several batches of the 100-km^3 postcaldera Early Rhyolite were calculated to have had 3–5 wt% H_2O (Waters and Lange, 2014). These were all CO_2-poor low-temperature (700–800 °C) biotite-bearing rhyolites characteristic of Long Valley.

At an intermediate stage of crystallization (30–50% crystals), interstitial melt and gas expelled from the crystal mush could ascend and accumulate as crystal-poor rhyolite near the top of the reservoir (Sisson and Bacon, 1999; Hildreth, 2004; Hildreth and Wilson, 2007); and such mush is itself commonly still mobile enough to erupt, typically drawn up in the wake of crystal-poor rhyolite in large zoned eruptions. Beyond 55–60% crystals, however, the mush passes a rheological locking point, locks up, and becomes a rigid, weakly permeable shell, which gradually thickens and solidifies into an impermeable granitic rind (Marsh, 1981; Lejeune and Richet, 1995). Some of the exsolving fluid may rise to the roof of the solidifying pluton through interconnected miarolitic cavities (Candela and Blevin, 1995), but for it to penetrate upward through a solid granite rind and the overlying country rocks would require some combination of confined fluid overpressure, thermoelastic cracking by cooling, and regional tectonic strain. The abundant recent earthquakes in and near Long Valley represent high-strain events that could shear any ductile shell enclosing the crystallizing residue, releasing pulses of aqueous fluid into the overlying hydrostatically pressured brittle zone (Fournier, 1999). And seismically induced fracture permeability could promote deeper penetration and circulation of hydrothermal fluids, enhancing cooling and volumetric contraction of the pluton lid, thereby promoting tensile cracking and still greater release of second-boiling fluids.

High viscosity of the rigidifying crystal sponge itself should impede pluton inflation, whereas second boiling would release an expanding fluid plume dispersed into a roof-rock fracture network where it could mix with meteoric hydrothermal waters.

At Long Valley today, the scenario proposed here envisages ascent of aqueous fluid expelled by second boiling at depths of 10–12 km from the nearly solid residue of the formerly enormous rhyolitic magma chamber. Long Valley has not been a system of small stocks or multiple porphyries like those envisaged beneath andesite-dacite stratovolcanoes or well-documented in studies of mineralized porphyries. It was, instead, a long-lived reservoir dominated by high-silica rhyolite, 10–20 km across and several kilometers thick, that had earlier released 650 km^3 of magma as the Bishop Tuff and ~100 km^3 of magma as the Early Rhyolite. It is the residue of this great reservoir that has for the last half-million years been crystallizing.

Geodetic or seismologic interpretation of processes associated with a batholith-scale rhyolite–granite pluton should not mistake such a system for the shorter-term behavioral patterns of intermediate stratovolcanoes or multi-intrusive porphyries. The spatial and time scales are drastically different.

Fluid ascending from the large crystallizing pluton provides a broad pressure source for ongoing uplift above the apex of the former magma chamber, beneath the resurgent dome, where vents for the postcaldera Early Rhyolite had been concentrated. The principal route for fluid egress toward the surface has developed unilaterally, only into the south moat ring-fault zone (Fig. 3), the wide and deep fracture network of which was recently reactivated by the regional tectonic stress manifest in the intense and sustained seismicity in the contiguous Sierra Nevada block (Fig. 4).

After summarizing the postcaldera eruptive sequence and the many inconclusive efforts to image a subcaldera magma body, I present below my geologically comprehensive perspectives on varied geophysical, volcanological, and tectonic observations that I find more consistent with fluid ascent than with intrusion of a new magma batch. Rather than overreliance on a geodetic model, I try to consider evidence from the entire geologic and magmatic history of the Long Valley region.

3. The Middle Pleistocene Long Valley magma chamber

Eruption of 650 km^3 of rhyolite magma as the Bishop Tuff at 767 ka was accompanied by collapse of Long Valley caldera. The area of deep structural subsidence inside the ring-fault zone (Hildreth, 2017) is an oval 12 by 22 km across (~210 km^2), representing only 50% of the ~420-km^2 floor of the topographic caldera depression (Fig. 3) but providing a minimum area for the magma chamber into which it collapsed. About 40 postcaldera eruptions of Early Rhyolite (750–640 ka), which is compositionally similar (but not identical) to the Bishop Tuff, produced ~100 km^3 of very crystal-poor lavas and tuffs that spread out over most of the caldera floor but issued from a multivent area no larger than ~75 km^2 in the west-central part of the caldera (Hildreth et al., 2017). It was this more focussed area of Early Rhyolite vents that was raised 400–500 m near the end of the Early Rhyolite episode by structural resurgence (between ~670 ka and 570 ka; Hildreth et al., 2017). And it is this circumscribed Early Rhyolite vent area, plausibly over the apex of

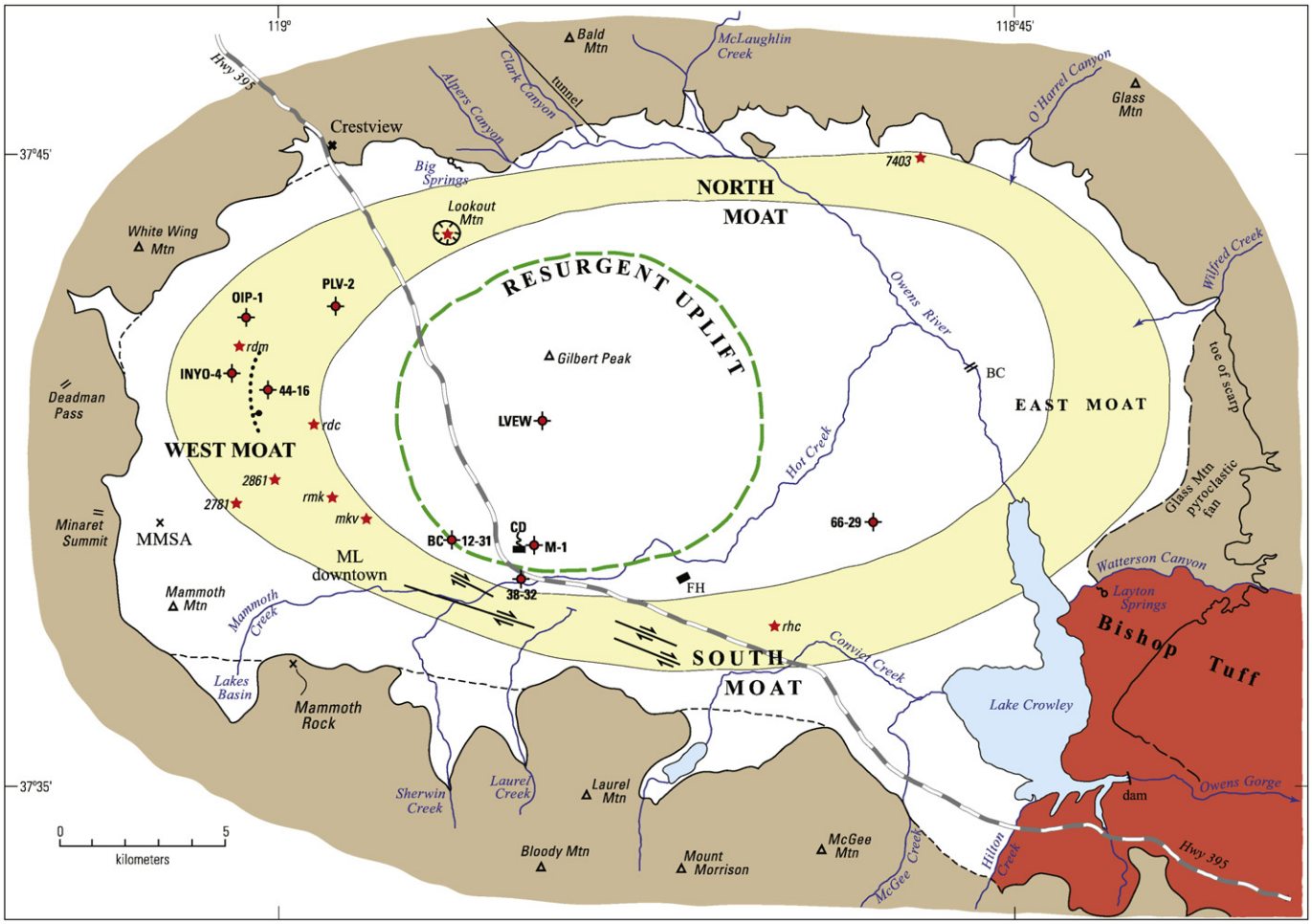

Fig. 3. Outline map of Long Valley caldera emphasizing its topographic wall, resurgent uplift, and structural ring-fault zone (yellow) between them. Precaldera rocks (brown), Cambrian to Pleistocene, form steep walls around 90% of the caldera periphery. To the southeast, Bishop Tuff ignimbrite outflow (red) filled the wide valley of precaldera Owens River, which had drained across the eastern part of the subsequent site of the caldera, from Clark Canyon into Neogene Owens Gorge. Dashed lines crossing caldera-wall embayments are meant to suggest continuity of basement rocks concealed beneath thin modern surficial deposits. Four concealed faults in south moat were inferred from seismicity (Prejean et al., 2002) and represent most of the South Moat Seismic Zone (see Fig. 4). Vent stars indicate selected postcaldera eruptive units (described in Hildreth and Fierstein, 2016a), conduits of which may have been influenced by the ring-fault zone: **mkv**, andesite of Knolls Vista; **rdc**, Dry Creek dome; **rdm**, Deer Mountain; **rhc**, Hot Creek flow; **rmk**, Mammoth Knolls dome; and Domes 2861, 2781, and 7403. Nine drillholes are identified: In south moat, M-1, 38–32, and BC 12–31 penetrated large slide masses of caldera-wall basement rocks that rest on intracaldera Bishop Tuff. In 3-km-deep LVEW, 1.2 km of Bishop Tuff is overlain by 622 m of Early Rhyolite and has been updomed ~400 m by structural resurgence (Hildreth et al., 2017). In 66–29, >1.5 km of Bishop Tuff is overlain by ~700 m of tuffaceous lake sediment. Wells 44–16, Inyo-4, OIP-1, and PLV-2 are discussed in Hildreth and Fierstein (2016a) and Hildreth (2017). Abbreviations: BC, Benton Crossing road bridge; CD, Casa Diablo geothermal plant; FH, fish hatchery; ML, town of Mammoth Lakes; MMS, Mammoth Mountain Ski Area (Main Lodge). Lake Crowley is a reservoir, dating from closure of Long Valley Dam in 1941, not a remnant of the middle Pleistocene caldera lake, which ultimately overflowed through the same outlet into Owens River Gorge (Hildreth and Fierstein, 2016b).

the middle Pleistocene magma reservoir, that has been subjected to 83 cm of uplift since 1980.

After the final Early Rhyolite eruptions (about 640 ka), there ensued an extended hiatus before the first of several episodic sets of Long Valley rhyolitic lavas (Fig. 1) erupted around the periphery of the resurgent uplift (Bailey, 1989). First was a crystal-rich chain of three small domes and one coulee (570–505 ka) that erupted through the northeast flank of the Early Rhyolite. Second was a set of six domes and flows (360–330 ka), in contact with caldera-lake sediment in the caldera's southeast moat, that exhibit a wide range in crystal content. Third was the crystal-rich 150-ka West Moat Coulee, and fourth was a set of three small crystal-rich domes (115–100-ka) in the west moat. The crystal-rich component of the compositionally mixed eruption of the Inyo Chain in 1350 C.E. is also residual Long Valley rhyolite (Reid et al., 1997). Altogether, the 15 units of younger Long Valley rhyolite add up to ~5 km^3, a small fraction of the 100 km^3 Early Rhyolite or of the 650 km^3 Bishop Tuff.

Despite the near-vertical structural grain of the stratified metamorphic rocks (Rinehart and Ross, 1964) that compose much of the foundered cauldron block (roof plate), and despite the complex system of faults transecting the resurgent uplift, there has not been a single eruptive leak on the uplift itself in the last half-million years. Volumetric eruption rate of postcaldera rhyolite was ~1 km^3/kyr for the 110,000-year-long Early Rhyolite interval, but it has been only ~0.008 km^3/kyr since 640 ka—a hundredfold decline.

The observation that all ~40 Early Rhyolite units are nearly identical in major-element composition (Hildreth et al., 2017) suggests that inmixing of unrelated or less evolved magma batches was trivial or absent during the 750–640 ka interval. Completion of most resurgence by 570 ka and absence of eruptions on the resurgently uplifted area after ~500 ka suggest that the pluton had become stably emplaced by then, thereafter crystallizing without further ascent.

Most of the 15 younger rhyolites (and all those younger than ~330 ka) were crystal-rich, low-temperature magmas (Bailey, 1978; Heumann, 1999; Heumann et al., 2002), which further suggests that large-scale separation of melt from crystal mush had ceased after eruption of the crystal-poor 333-ka Hot Creek flow. Abundant evidence that the Long Valley rhyolitic system is moribund and that the mantle-driven magmatic focus had shifted southwestward by ~230 ka to the extracaldera Mammoth Mountain trachybasalt-trachydacite volcanic

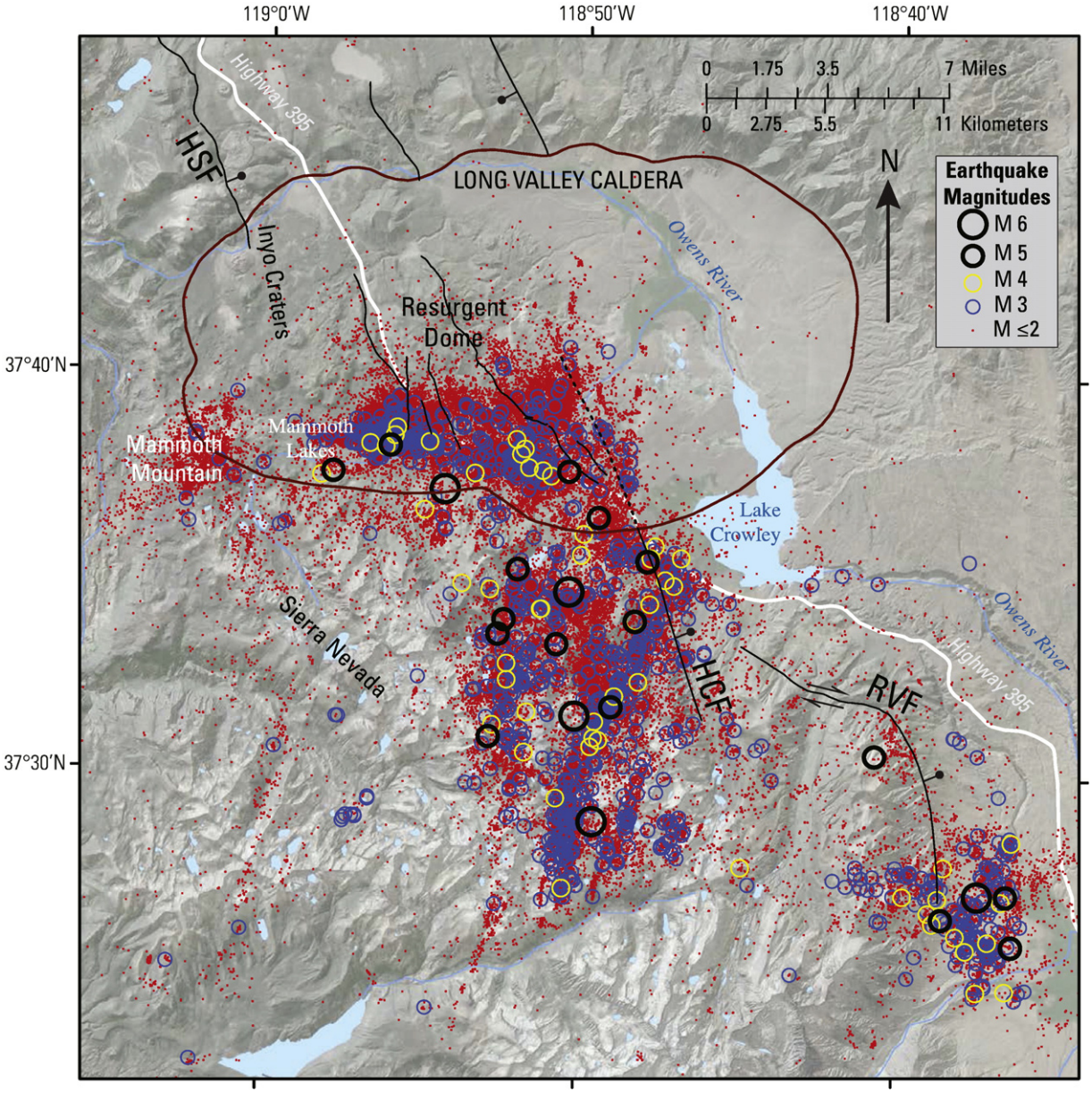

Fig. 4. Map of epicenters for earthquakes with magnitudes $1.5 \geq M \leq 6.5$ from 1987 to 2014, scaled by symbol size; figure adapted from Hill et al. (2016). Contiguity of seismogenic domains in caldera's south moat ring-fault zone and in extracaldera Sierra Nevada is apparent, while those around Mammoth Mountain and Round Valley (to southeast) are separated. Epicenters for the 1978–1983 interval (prior to installation of the locally dense seismic network in 1984) are from standard NCSN catalog and include only $M \geq 3$ earthquakes. Epicenters for $M \geq 1$ earthquakes in 1984–2014 interval are from double-difference catalog of Waldhauser (2009). Abbreviations: HCF, Hilton Creek fault (dotted where beheaded, deactivated, and buried by caldera collapse); HSF, Hartley Springs fault; RVF, Round Valley fault.

field was summarized by Hildreth et al. (2014) and Hildreth and Fierstein (2016a).

4. Unsuccessful attempts to image a contemporary Long Valley magma chamber

Several teleseismic tomographic experiments and at least a dozen more using local earthquakes have attempted to image a contemporary magma body under Long Valley. Although most studies claimed to have identified low-velocity or attenuation domains—scattered at widely varied depths and locations, none unambiguously imaged a magma chamber (Steeples and Iyer, 1976; Sanders, 1984; Luetgert and Mooney, 1985; Elbring and Rundle, 1986; Dawson et al., 1990; Steck and Prothero, 1994; Sanders et al., 1995; Weiland et al., 1995). Nearly all hedged their interpretations of the perceived anomalies as, alternatively, hot rock, partial melt, or hydrothermal fluids, although some portrayed cartoons of grandiose magma bodies. In retrospect, ray paths from local earthquakes to local stations seem inadequate to illuminate the present-day inflation domain; and the wavelengths used in teleseismic tomography are too long to image a small magma body. Among the conclusions of the many Long Valley experiments were the following.

Kissling (1988) used high-resolution tomography based on local earthquakes to derive a 3-dimensional P-wave velocity model of the Long Valley region. Although he noted a zone of slightly low P-wave velocity (−3%) at depths of 3–7 km beneath the south moat and southern fringe of the resurgent dome, his principal conclusion was the "apparent absence of a large contemporaneous magma chamber at midcrustal level beneath Long Valley caldera." His low-velocity domain is exactly where Prejean et al. (2002) later identified ascending earthquake swarms interpreted as fluid pressure pulses caused by low-viscosity aqueous fluid rising rapidly from depths of ~10 km.

Hauksson (1988) scrutinized high-quality records from a borehole seismometer and from surface clusters of instruments on opposite sides of the resurgent dome. He found "no conclusive evidence for shadowing or anomalous attenuation of S waves in the downhole seismograms", no systematic travel-time delays, and no systematic variation with depth in *Vp*/*Vs* ratio. Although the data were specifically collected to provide evidence about possible magma chambers, he concluded that the absence of evidence for a magma chamber is a "fundamental observation." He suggested that S-wave shadowing observed by others could be explained by radiation pattern effects.

Black et al. (1991) conducted wide-angle and vertical-incidence seismic reflection profiling in 1984–1985 in the northwest part of the caldera, specifically targeting a northwestern S-wave-attenuating zone (Sanders, 1984), where Hill (1976) had first identified a deep reflector. Despite degradation of data quality by the complex near-surface caldera fill, they concluded that there is "little or no evidence that strong magma reflectors exist in the areas expected from previous studies." They reinterpreted what had been thought to be intra-basement reflectors as reflections from buried fault scarps (which are very likely in that sector, probably representing precaldera relay ramps in the left-stepping subcaldera transfer zone of the rangefront fault system).

Romero et al. (1993) installed a special fan array of 3-component borehole receivers to conduct a high-resolution tomographic study, targeting the purported magma chamber beneath the resurgent dome and based on 280 well-distributed local earthquakes in 1989–1990. No distinct low-velocity anomaly was identified, although a diffuse zone of slightly reduced velocity persisted to a depth of ~8 km, which they attributed to fracturing and hydrothermal alteration. This is where second-boiling fluids ascending from the apex of the moribund rhyolite reservoir would be expected to utilize and promote a fracture network. Normal to low *Vp*/*Vs* ratios and the lack of an S-wave anomaly were cited as evidence "against the presence of a sizable and distinct magma body at shallow to midcrustal depths beneath Long Valley caldera."

Foulger et al. (2003) performed a tomographic inversion for the western half of the caldera, based on thousands of local earthquakes recorded by a temporary 1997 array of 69 three-component seismic stations. Low wave speeds were restricted to the southern part of the resurgent dome at depths of 4–5 km, and the base of the seismogenic zone was found to deepen eastward across the resurgent dome from ~5 to ~8 km. They stated that "magma may be ruled out as an explanation for the low-*Vp* anomalies beneath the western and southern portions of the resurgent dome…because this would be expected to be characterized by high *Vp*/*Vs* anomalies, which are not observed, as well as by elevated temperatures at 3 km depth." From 2 to 3 km depth beneath the resurgent uplift, measured temperature was isothermal at 100 °C in Well LVEW.

Sanders (1993) and Ponko and Sanders (1994) tested the limits of what could be detected with the available seismic coverage. They selected high-quality 3-component seismograms from ~100 local earthquakes in order to tomographically invert for 3-dimensional P- and S-wave differential attenuation structure in the upper crust beneath the caldera. At a depth of 7–8 km beneath the south edge of the resurgent dome, they identified a zone of S-wave attenuation, which they speculated "may represent the top of a central Long Valley magma chamber." Two areas of high P-wave attenuation were identified—one above the S-wave anomaly at depths of 6–7 km, the other at 4–5 km beneath the east flank of Mammoth Mountain. Lacking S-wave attenuation, the two areas were interpreted not as magma but as fractured rock containing supercritical hydrothermal fluids. Their 7–8 km zone of S-wave attenuation is precisely where Prejean et al. (2002) later identified an intricate fabric of faults that extend to depths of 10 km and are defined by upward-migrating earthquake swarms activated by fluid-pressure transients caused by rapid ascent of low-viscosity aqueous fluid, not magma.

A special issue of *Journal of Volcanology and Geothermal Research* in 2003 assembled ten papers concerned with unrest at Long Valley caldera, but there was hardly a mention of "magma chambers." Attention had by then turned to shallow geothermal fluid flow from the west moat, episodes of seismic unrest, and modeling of the ~80 cm uplift in the interval 1975–1999. Farrar et al. (2003) concluded that "information from LVEW and other wells in the region indicates that a large, long-lived magma chamber is unlikely to exist beneath the resurgent dome."

4.1. Latest seismic tomographic experiments

After research well LVEW atop the resurgent dome (Fig. 1) recorded a temperature of 103 °C at its bottom depth of 3000 m, and after the failure or ambiguity of so many tomographic attempts to identify a magma body, most investigators abandoned the formerly prevalent model of a great contemporary chamber. Nonetheless, a decade later two new tomographic searches for magma beneath the caldera were undertaken by Seccia et al. (2011) and Lin (2015). Using local earthquakes, the former team created a tomographic *Vp* model, complemented by a teleseismic receiver function model based on two permanent broadband stations SE and SW of the resurgent dome. They inferred the three following features. (1) a *high-Vp* anomaly ~3 km wide beneath the resurgent dome at depths of 1–5 km. This is precisely where Elbring and Rundle (1986) had claimed to have imaged a magma body at a depth of 3.7 km. (2) A WNW-trending low-*Vp* anomaly as long as 17 km at 6–7 km depths, extending beneath the resurgent dome but also as far as Hot Creek and Lake Crowley; about half of the anomaly thus lies east of the uplifted area. (3) A broader low-velocity volume ~20 km wide and 8–14 km deep, underlying much of the caldera. The authors speculated whether anomaly (2), with *Vp* reduction of 8–10%, could represent interstitial fluids or 2–3% partial melt. They also speculated that the deeper anomaly (3), with *Vp* reduction of ~5% and much greater *Vs* reduction, might contain tens of percent partial melt, but Lin's (2015) results conflict with that suggestion.

Lin (2015) combined a new 3-D velocity model and high-precision locations of (1984–2014) local earthquakes to derive simultaneously resolved *Vp* and *Vp*/*Vs* tomographic models for the caldera and vicinity. For the south moat ring-fault zone, low *Vp* was recorded at all depths (0–10 km), and high *Vp*/*Vs* values at 1–3 km depths were attributed to hydrothermal fluids. Beneath the resurgent dome, high *Vp* and low *Vp*/*Vs* values were identified from the surface to a depth of ~4 km, in accord with Seccia et al. (2011). Beneath that, an aseismic domain 4.2–6.2 km deep with medium *Vp* and high *Vp*/*Vs* was offered as a candidate for containing partial melt, but this is only 1200 m directly below the 103 °C bottom of the LVEW well and might alternatively represent a gas-water mixture. Still deeper at 6.2–8.4 km, Lin identified a layer with high *Vp and* high *Vp*/*Vs*, which she speculated might contain dense cumulates, which are implausible in a high-silica rhyolitic magma system. The still-deeper low-*Vp* domain at depths below 8 km inferred by Seccia et al. (2011) turned out to have low *Vp*/*Vs* values, "inconsistent with the presence of partial melt" (Lin, 2015, p. 28). The deep low-*Vp*/*Vs* region may instead represent pressurized gas-bearing rock with high fluid compressibility.

In summary, even with the latest methods, no magma body has been imaged. Most or all of the velocity anomalies are more plausibly attributed to hydrothermal fluid than to magma.

5. Late Pleistocene magmatism limited to Mammoth system and west moat

The Mammoth basalt-to-dacite system started up ~230 ka, erupting through pre-Cenozoic basement just outside the structural caldera (Fig. 5). It consists of a central dacite edifice— Mammoth Mountain (100–50 ka)—and ~38 peripheral units that include basalt, andesite, and dacite (230–8 ka). The Mammoth system is consistently more alkalic than the rhyolitic Long Valley and Mono Craters systems (Fig. 6), and it includes no rhyolite. All 25 eruptive units that built the Mammoth

Mountain edifice were glacially scoured during MIS 2, and the central edifice has been inactive for the last 50 kyr (Hildreth and Fierstein, 2016a). The peripheral, generally more mafic, system has erupted roughly every 10,000 years from its inception (~230 ka) through to the Red Cones eruption of 8 ka (Hildreth et al., 2014). Widespread and continuous discharge of magmatic CO_2, He-isotope ratios as high as 6.7 Ra, and seismicity extending from the edifice to lower-crustal depths of 30 km (Shelly and Hill, 2011) attest to a magmatically active mantle beneath the Mammoth system, probably to basaltic injection of the lower crust, and certainly to release of a volatile phase from CO_2-saturated basalt. Equivalent evidence of active or late Pleistocene magmatism beneath most of Long Valley caldera is absent—except beneath its west moat.

5.1. Residual magma only beneath the west moat

The west moat is contiguous with the active Mammoth system, and I infer that the thermal contributions of mantle-derived Mammoth basalts that have intruded into or near the caldera's ring-fault zone have been responsible for delaying crystallization of the Long Valley rhyolite beneath the west most. Rhyolitic eruptions took place in the west moat at approximately 150, 115, 110, and 100 ka (Hildreth and Fierstein,

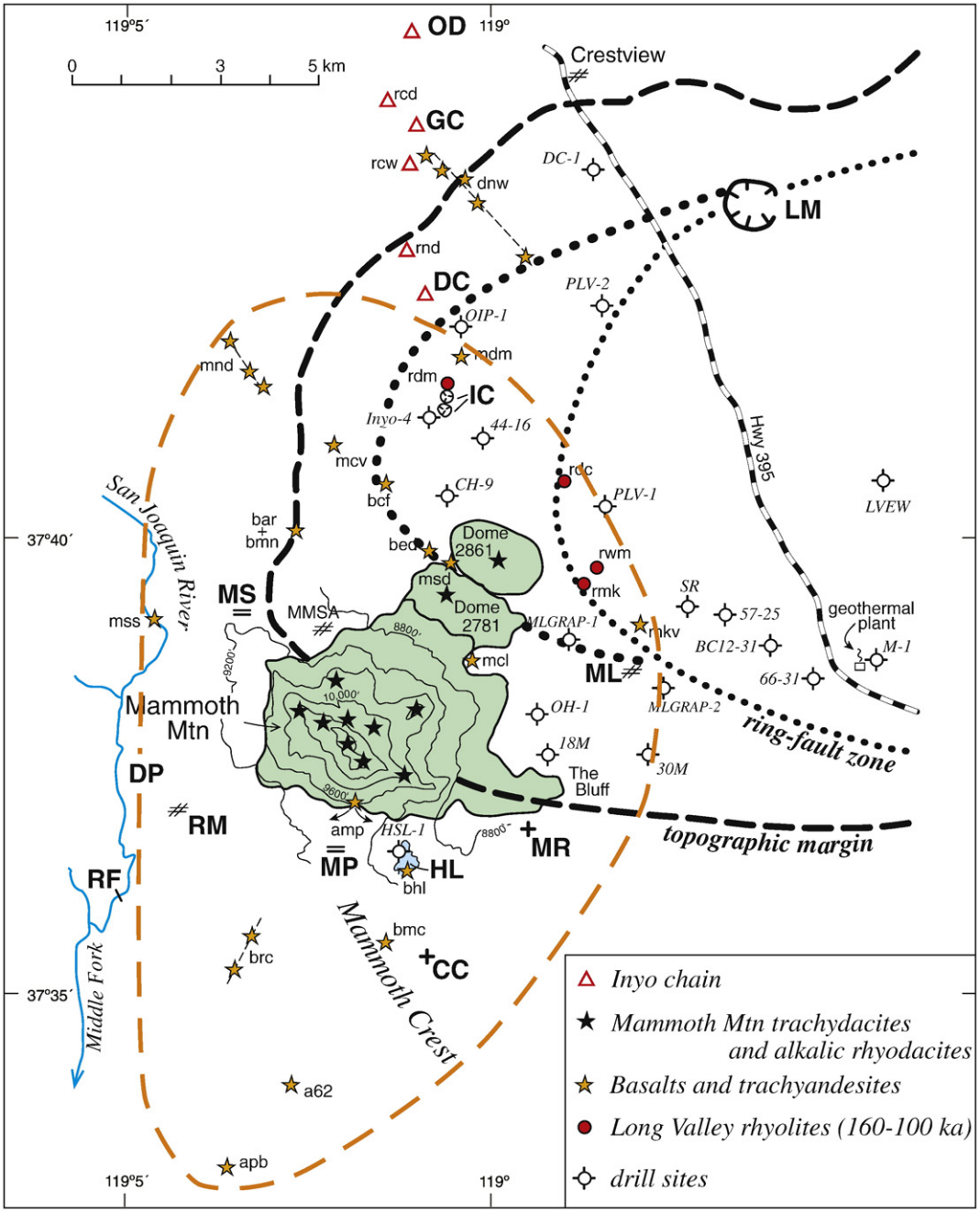

Fig. 5. Distribution of volcanic vents exposed on and near Mammoth Mountain at southwest margin of Long Valley caldera. Mammoth Mountain edifice is colored green, and its exposed vents are indicated by black stars. Peripheral mafic and intermediate vents are represented by orange stars. Four Long Valley rhyolites (150–100 ka) contemporaneous with the alkaline Mammoth system are indicated by red dots in caldera's west moat. Red open triangles represent Holocene rhyolitic Inyo chain; of these, those indicated by bold letters erupted in 1350 C.E.—OD, Obsidian Dome, GC, Glass Creek flow, DC, Deadman Creek flow, IC, Inyo (phreatic) Craters. All other vents are identified by 3-letter unit labels employed and described at length by Hildreth and Fierstein (2016a). Logs for drillholes located on map are given in Fig. 14 of Hildreth and Fierstein (2016a). Other abbreviations: CC, Crystal Crag; DP, Devils Postpile; HL, Horseshoe Lake; LM, Lookout Mountain; ML, downtown Mammoth Lakes; MP, Mammoth Pass; MR, Mammoth Rock; MS, Minaret Summit; RF, Rainbow Falls; RM, Reds Meadow.

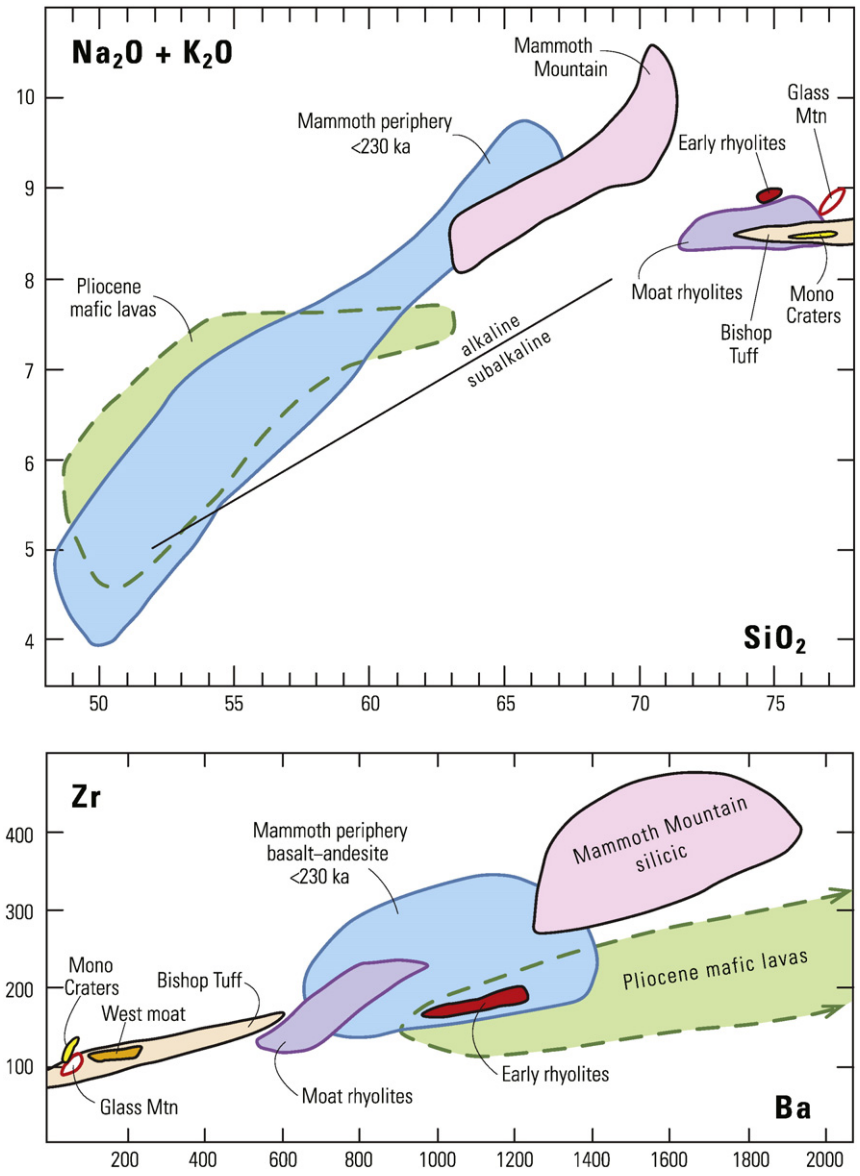

Fig. 6. Total alkalies ($Na_2O + K_2O$) *versus* SiO_2 contents in weight percent for Mammoth Mountain dacite dome complex and peripheral units of wider Mammoth magmatic system (Fig. 5), emphasizing distinction from rhyolites of Long Valley and Mono Craters. Four rhyolite extrusions in west moat (Fig. 1) that erupted 150–100 ka may have been thermally sustained by the adjacent and contemporaneous Mammoth system, but they were not materially affected by it. Bishop Tuff data from Hildreth and Wilson (2007); Glass Mountain data from Metz and Mahood (1985, 1991); Mono Craters data from Kelleher and Cameron (1990); Early Rhyolite data from Hildreth et al. (2017); Mammoth, Pliocene, and Moat data from Hildreth and Fierstein (2016a). Divider between alkaline and subalkaline fields after LeBas et al. (1986).

2016a). Elsewhere in the caldera, the final eruptions were at 360–330 ka, exclusively rhyolitic. In and near the ring-fault zone contiguous with the west moat, Mammoth system eruptions of basaltic to trachyandesitic magma (Fig. 5) took place at about 235–220, 190–180, 175, 172, 165, 164, 154, 160–150, 131, 125, 101, 90, 85, 66, 33, and 17 ka (Hildreth and Fierstein, 2016a). As there has been no late Pleistocene (130–11 ka) magmatism of any kind anywhere else in the caldera, it seems a strong inference that the extracaldera mafic Mammoth magmatism has sustained or reactivated pods of Long Valley rhyolite in the contiguous west moat (and only in the west moat).

The youngest units that vented unequivocally inside the west moat (Hildreth and Fierstein, 2016a) were (1) a chain of hybrid, variably mingled rhyodacite-andesite lavas that yield ages of 40–27 ka and include a quartz-bearing rhyolite contribution; (2) a large mafic scoria cone and derivative lava field that erupted ~33 ka; and (3) the compositionally mingled rhyolite–rhyodacite Deadman Creek flow of 1350 C.E. The crystal-rich phase of the late Holocene mingled unit is mineralogically and chemically consistent with being residual Long Valley rhyolitic crystal mush (with up to 40% phenocrysts). The crystal-poor phase appears to be Mono Basin magma (with only 2–3% phenocrysts) that advanced southward as a dike along the rangefront fault system and entrained some of the Long Valley rhyolitic mush (Sampson and Cameron, 1987). The mingled Holocene flow also contains chilled mafic magmatic enclaves as big as 10 cm, heavily contaminated by crystals from the host rhyolite (Varga et al., 1990), thus verifying the recent presence of mafic as well as rhyolitic magma in storage beneath the west most.

The 1350 C.E. Deadman Creek flow shares with the nearly identical phenocryst-rich rhyolite of the adjacent 115-ka rhyolite dome of Deer Mountain a suite of zircons that yield crystallization model ages of ~230 ka (Reid et al., 1997). It is unlikely to be fortuitous that the ~233-ka inception of mafic magmatism in the greater Mammoth system coincides with the 230-ka clusters of zircon ages. Mammoth mafic magmatism evidently reactivated west moat rhyolite, promoting resorption of older zircons. After subsequent cooling, however, the newly precipitated 230-ka suite of zircons has endured into recent time and has been tapped twice, at 115 ka and in 1350 C.E. Zircon

saturation temperatures and coexisting Fe-Ti oxide temperatures for these lavas are both close to 800 °C, implying, on the one hand, that these low-temperature crystal-rich rhyolites have never been strongly reheated, but, on the other hand, that mafic magma replenishment at a deeper level has been thermally effective for 230,000 years in preventing complete crystallization. Both of these west moat rhyolites are extraordinarily rich in phenocrysts, not far from the locking point, and may have needed disturbance by unrelated magma batches to have erupted at all.

Adjacent to Deer Mountain, geothermal well 44–16 (Figs. 3, 5) was found to be as hot as 213 °C (Suemnicht, 1987) and produces a vigorous flux of CO_2, which makes a major contribution to the ~95 tonnes/day of CO_2 carried eastward from the west moat along the shallow geothermal aquifer that surfaces at Casa Diablo and Hot Creek. As at Mammoth Mountain, the CO_2 flux certainly arises from cryptic basalt, not from residual rhyolite (in which CO_2 solubility is low). Hill (1976) and Peacock et al. (2016) inferred magma storage beneath the west moat, based on seismic reflection and magnetotelluric evidence, respectively. The eruptive and petrologic evidence is compelling that they are right. No comparable sets of complementary evidence for surviving magma have been found anywhere else beneath the caldera.

6. Seismicity in the Sierra Nevada directly adjacent to Long Valley's south moat

The South Moat Seismic Zone (SMSZ) extends about 12 km along the caldera's ring-fault zone, bounded by the Pleistocene resurgent dome to the north and a large contiguous seismogenic domain in the Sierra Nevada to the south (Fig. 4). The Sierran and SMSZ areas of dense seismicity are continuous, not spatially discrete, whereas the seismically active areas at Mammoth Mountain (to the west) and Round Valley (to the southeast) are geographically separate. Around most of the ring-fault zone and beneath most of the resurgent dome, seismicity is negligible. Major seismicity in the adjacent Sierra started in 1978 and has persisted ever since, more continuously than the recurrent swarms in the SMSZ (Fig. 7 of Hill, 2006). Four *M*6 earthquakes in May 1980, three of which were in the Sierra and the other in the ring-fault zone, marked the onset of recurrent seismic swarms along the SMSZ. Fumaroles and hot springs along the south moat had been well known since settlement in the 1870s, but south-moat seismicity began abruptly only after the big Sierran earthquakes of May 1980 and was thus evidently triggered tectonically. I infer that the Sierran earthquakes reactivated the directly contiguous segment of the steeply dipping ring-fault zone (which had been there since 767 ka), initiating what soon became known as the SMSZ. It was only this short segment of the ring-fault zone, shaken by the adjacent Sierran seismicity and subject in common to the same regional tectonic stressfield (Prejean et al., 2002; Hill, 2006) that became seismically active after May 1980, not the other 300° of the aseismic ring-fault zone, the 75-km-long circumference of which encircles the equally aseismic resurgent uplift.

During the interval 1980–2015, there were ~720 earthquakes greater than *M*3 in the caldera and ~1140 greater than *M*3 in the adjacent Sierran block—within a seismogenic volume larger than that within the caldera but beneath an area smaller than the caldera itself (Fig. 4). Cumulative seismic moments for the 35-year interval were 2.4×10^{18} N-m in the caldera and 8.7×10^{18} N-m in the Sierra. There have thus been ~1.6 times more $M > 3$ events in the Sierra and ~3.6 times more seismic energy released in the Sierra than in the adjacent caldera. Caldera hypocenters, nearly all in the south moat ring-fault zone, are distributed continuously at depths from ~3 km to 10 km. Hypocenters in the adjacent Sierran block are likewise mostly distributed between 3 and 10 km but also extend as deep as 15 km (Prejean et al., 2002), probably reflecting colder and drier extracaldera basement that produces a deeper brittle-ductile transition.

Neither the distribution of SMSZ earthquakes nor their focal mechanisms are consistent with the quasi-circular symmetry of the ongoing uplift shown by geodetic data. Prejean et al. (2002) concluded that the stresses promoting intracaldera inflation have little effect on the regional tectonic stressfield that dominates SMSZ seismicity. Moreover, inflation of the uplift could be expected to impart stresses that would impede the dextral slip inferred by Prejean et al. (2002) along the SMSZ. If seismicity in *both* the Sierra and the SMSZ reflects regional tectonic stresses (as concluded by Prejean et al., 2002), and if SMSZ seismicity is mediated and modulated by pressurized geothermal fluids (Hill, 2006), then, as most of the Pleistocene resurgent structure (and indeed most of the rest of the caldera) is seismically quiescent, is not the prime mover clearly the extracaldera tectonic stress field?

Cumulative uplift of ~83 cm since 1980 is centered in the south-central part of the Pleistocene resurgent structure, which was upwarped at least 400 m by early postcaldera resurgence (largely accomplished by 570 ka; Hildreth et al., 2017). The recent uplift was marked by pulses of more rapid rise in 1980, 1982, 1983, 1989–90, and 1997–98 (Hill et al., 2002; Hill, 2006) plus a weak resumption of uplift since 2011 (Montgomery-Brown et al., 2015). Setting aside the question of which may have triggered which (Hill et al., 2003), all the pulses of uplift have overlapped in time with extended episodes of seismicity in both the Sierra and the SMSZ (Hill, 2006). Much of the 1989 seismicity took place under Mammoth Mountain, which is in the Sierra, on granitic basement, not in the caldera. If intracaldera uplift, inboard of the ring-fault zone, were really the main cause of the seismicity, why does this recurrent linkage to the Sierra occur and why are most of the earthquakes and most of the seismic moment in the extracaldera Sierra Nevada block?

7. South moat seismic zone

Within the caldera, a vast number of earthquakes occurs at depths of 3–10 km in the SMSZ (mostly 4–9 km; Prejean et al., 2002), which extends principally for 12 km along the caldera's ring-fault zone but also encroaches slightly northward under the southernmost fringe of the Pleistocene resurgent structure (Fig. 4), which had been updomed 400–500 m by 570 ka. The seismically active southern fringe of the old uplifted area is largely coincident with a strip where fumaroles are a manifestation of geothermal fluids. Fumaroles and earthquakes are jointly most concentrated in two lobes—around Fumarole Valley and around the site of Casa Diablo Hot Springs (Figs. 1, 4)—the two areas where uplift-crossing grabens join the south moat ring-fault zone. The seismically active fringe also extends 2–3 km around the southeast foot of the uplift as far as Little Hot Creek (Fig. 1), which is likewise an area of fumaroles and hot springs. The southeastern features are inferred to overlie a deeply buried segment of a north-trending precaldera fault (Fig. 4) that was beheaded and deactivated by the caldera collapse and has had little or no postcaldera surface displacement.

The geothermal aquifer is not sourced in the SMSZ or beneath the uplift but, instead, flows eastward along the seismically active strip from sources in the caldera's west moat (Sorey et al., 1991; Suemnicht et al., 2006). Although the aquifer itself flows through the 1–2-km-thick caldera fill, high-resolution hypocenter relocations (Prejean et al., 2002; Shelly et al., 2016) have identified dense seismicity below the aquifer that defines cryptic sets of faults that extend to depths of 8–10 km beneath the SMSZ and to 7.5 km beneath the Blue Chert area (Fig. 1) at the southeast fringe of the old structural uplift. Seismicity beneath the SMSZ aquifer is within the caldera's ring-fault zone, and it may extend deeper than the subsided roof plate, down along what had been the subjacent sidewall of the precollapse magma reservoir to depths of 10–12 km (Fig. 7). Earthquake swarms that define the north-trending fault set inferred by Shelly et al. (2016) near Blue Chert may coincide with a concealed northern segment of the Hilton Creek fault that was beheaded by the caldera collapse (Fig. 4).

The intracaldera seismic zone is defined by upward-migrating earthquake swarms that are thought to be activated by elevated fluid-pressure transients caused by rapid ascent of low-viscosity aqueous fluid

(Shelly et al., 2016). The source of such ascending fluid could be "second boiling" of the crystallizing residue of the former Long Valley rhyolitic magma reservoir at depths of 10 km or more beneath the nearby area of recent uplift. Tectonically reactivated expulsion of (dominantly aqueous, CO_2-poor) volatile components from the moribund rhyolite, which is finally solidifying to granite, pressurizes the long-established resurgent flexure and escapes laterally to the newly shattered segment of the ring-fault zone in the south moat (Fig. 7). There is no evidence for *any* magma beneath the SMSZ, nor is there any evidence for *new* magmatic intrusion beneath the uplift or anywhere else east of the west moat.

None of the cryptic faults inferred by the high-precision hypocenter relocation studies, neither in the caldera nor in the Sierran block, are known to have surface expression (Prejean et al., 2002; Hill, 2006; Shelly et al., 2016). Slip on at least one of the cryptic dextral faults inferred by Prejean et al. (2002) appears to have begun in 1997. Since none of them has yet broken the surface, perhaps all are young, having been initiated or reactivated by the quartet of *M*6 shocks in 1980.

If fluid ascent is the key to uplift, as inferred in the present analysis, then increments of uplift might well be expected to precede onset of SMSZ seismic swarms, as sometimes recorded (Hill et al., 2003; Hill, 2006), owing to the additional time required for each fluid pulse to escape laterally from beneath the uplift toward the reactivated ring-fault segment nearby. Comparable time lags are recorded at Campi Flegrei caldera (Italy) where recurrent episodes of uplift attributed to pressurization of the hydrothermal system are followed by spikes in CO_2 and He emissions and accompanying seismicity many months later (Chiodini et al., 2015).

Earthquakes are rare beneath most of the resurgent structure, as well as on its west, north, and northeast flanks (Fig. 4) where geothermal fluids, if present, have no surface manifestations. Beneath most of the Pleistocene resurgent uplift, there is no elevated heat flow (in wells) and very little seismicity. Why would an ongoing intrusion, as advocated by some, not be accompanied by earthquakes under the old cold resurgent structure or around most of the encircling ring-fault zone?

8. Resurgence, magmatism, and ascending fluid

Intracaldera Bishop Tuff, >1100 m thick beneath the uplift, was updomed >400 m (Fig. 8), partly by intrusion of Early Rhyolite sills or laccoliths into the ignimbrite (McConnell et al., 1995), apparently near the end of the Early Rhyolite eruptive sequence (750–640 ka) or soon thereafter (Hildreth et al., 2017). Several of the Early Rhyolite lavas were perlitized by flowing into the caldera lake, necessarily before being structurally uplifted far above any shoreline of the lake. Ice-rafted erratics from the Sierra Nevada were dropped or beached on west-facing 700-ka Early Rhyolite lavas and later raised 200–300 m above nearby highstand shorelines of the caldera lake, thus confirming that resurgent uplift took place predominantly late in (and after) the Early Rhyolite eruptive interval. A 700-ka Early Rhyolite lava flow moved southeastward from Lookout Mountain across an area that only later became part of the uplift (Fig. 1). But an adjacent 570-ka Moat Rhyolite lava flow poured steeply down the north slope of the resurgent uplift into the caldera's north moat (Fig. 1). Most of the uplift is thus inferred

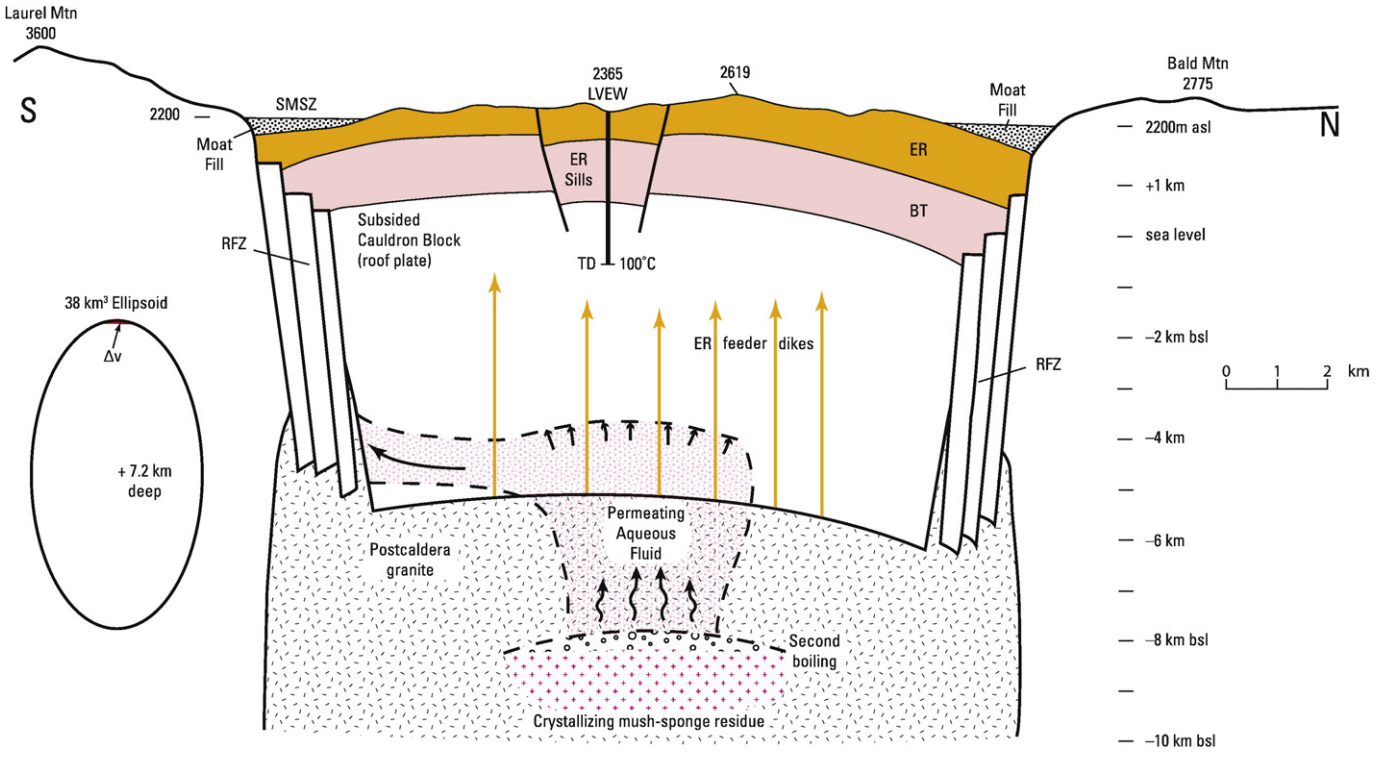

Fig. 7. Schematic north-south cross-section of 16-km-wide Long Valley caldera, depicting pressure source for ongoing uplift as aqueous fluid released by second boiling of late-stage crystallizing residue of formerly large rhyolitic magma chamber. Ring-fault zone (RFZ) encloses subsided roof plate of Sierran basement rocks ~6 km thick. Intracaldera Bishop Tuff (BT; 767 ka) totals ~350 km^3, and postcaldera Early Rhyolite (ER; 750–640 ka) totals ~100 km^3; both were bent upward by caldera resurgence, most of which took place 670–570 ka. ER erupted at several vents clustered on what later became the resurgent dome; their feeders are depicted arbitrarily as dikes, and ten ER sills that intrude the Bishop Tuff are shown in Fig. 8. Well LVEW atop the resurgent dome was cored to a total depth (TD) of 3000 m, where temperature was 100 °C. CO_2-poor aqueous fluid escapes laterally to South Moat Seismic Zone (SMSZ), a 12-km-long segment of RFZ recently activated by regional tectonic seismicity; remainder of RFZ is aseismic, while SMSZ experiences recurrent fluid-mediated seismic swarms. At left, an equivalent of 38-km^3 ellipsoidal pressure source modeled beneath resurgent dome by Montgomery-Brown et al. (2015) is depicted at same scale, along with its 2011–2014 calculated volume increment (at its top in red) of 0.06%. No vertical exaggeration. Elevations in meters and in kilometers above and below sea level.

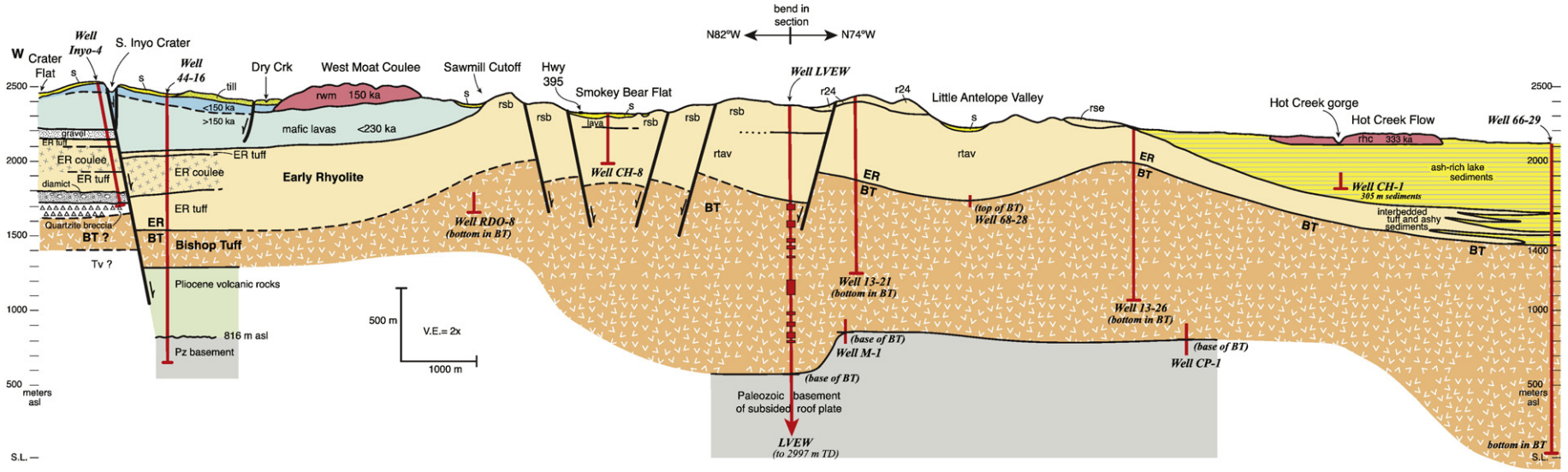

Fig. 8. West-east geologic cross-section spanning Long Valley's resurgent uplift. Elevations are in meters above sea level. Vertical exaggeration is twofold (2×). There is an 8° bend in section at Well LVEW, from 98° in the west to 106° in the east. Seven wells drilled on or close to the line of section are plotted. Data from several additional wells 1–3.6 km from the line of section helped inform extrapolation of contacts at depth. For example, base of Bishop Tuff (BT) is indicated for Well M-1, which lies 3.6 km south of the section, and for Well CP-1, which lies 2.2 km north of it; 305-m-deep Well CH-1 lies 2 km north of the section and is entirely in tuffaceous lake sediments. All well logs are depicted in Hildreth and Fierstein (2016a) or Hildreth et al. (2017). Ten sills of Early Rhyolite composition are indicated in red in Well LVEW, intruding the BT at depths given by McConnell et al. (1995), nearly central beneath the uplift. Sills were not encountered in other wells. Units **rsb**, **rse**, **r24**, and **rtav** are Early Rhyolite (ER) eruptive subunits described by Hildreth et al. (2017). Units **rhc** and **rwm** are younger (post-ER) rhyolite lava flows in the caldera moat, described by Hildreth and Fierstein (2016a). **S**, surficial deposits. Relatively shallow depth of Bishop Tuff in Well 13–26 is anomalous, suggesting unexposed structure discussed by Hildreth et al. (2017). For interpretation of caldera-wall avalanche deposit in Well Inyo–4, see Hildreth (2017) and Hildreth et al. (2017).

to have taken place after ~670 ka and to have been complete by 570 ka, thus within a 100,000-year interval that was long after the 767-ka caldera-forming eruption.

Nonetheless, lesser amounts of uplift did take place later, probably episodically. Where it impinges on the resurgent structure, the northwest margin of the 333-ka Hot Creek rhyolite coulee was bent upward by ~40 m (Hildreth and Fierstein, 2016a, 2016b). Several mafic lavas ($^{40}Ar/^{39}Ar$-dated from 180 ka to 125 ka) that flowed eastward from vents in the west moat are cut by graben faults that cross the uplift, but the vertical displacements are limited to only 10–30 m (Hildreth and Fierstein, 2016a); the faulting nonetheless indicates that intermittent increments of lesser uplift continued into the late Pleistocene, long after the final eruptions on or near the resurgent dome. After 500 ka, volcanism was limited to moats peripheral to the uplift, and nothing more erupted through the resurgent dome (Fig. 1). The dome structure is older than 570 ka, but small increments of uplift, unrelated to eruption, have persisted intermittently.

It seems probable that the ~83 cm of cumulative episodic uplift since 1980 likewise represents incremental structural accentuation of the longstanding domical flexure (Figs. 7, 8) by pressurization from below, rather than a wholly new bending of the roof plate. Ongoing ascent of low-viscosity aqueous fluid sourced as deep as 10 km around the southern fringe of the uplift has been invoked to explain the consistently upward-propagating earthquake swarms in the SMSZ (Prejean et al., 2002; Shelly et al., 2016). The ascending fluid may provide the principal pressure source centered beneath the Pleistocene uplift itself, whence some of the fluid escapes laterally to the SMSZ (Fig. 7).

Hurwitz et al. (2007) modeled conditions under which the poroelastic response to increasing fluid pressure and accompanying thermoelastic rock expansion could promote intracaldera uplift. Their numerical simulations were extended by Hutnak et al. (2009), who showed that dual-phase liquid-gas hydrothermal flow can, by a combination of pore-pressure transients and longer-term thermal expansion, produce large-scale uplift on timescales ranging from annual to millennial.

These studies noted that subsequent dwindling of fluid pressure or abrupt increases in permeability by hydrofracturing could induce subsidence. An episode of slight subsidence was indeed recorded at Long Valley in 1998–2002 (Langbein, 2003). The absence, so far, of larger subsidence episodes might be related to (1) the restricted, unilaterally southward, fluid-escape path; (2) an extended interval of recently triggered pulses of fluid ascent from the large plutonic reservoir; or (3) the weakness of upper-crustal hydrothermal circulation beneath most of the uplift, in contrast to restless calderas at Yellowstone and Campi Flegrei where vigorous system-wide convection hastens cooling and subsidence.

The lower limit of SMSZ seismicity at 9–10 km may reveal the depth at which fluids released by second boiling from the residue of Long Valley's formerly large rhyolitic chamber, now finally crystallizing to granite, emerge from the ductile zone into parts of the ring-fault zone capable of brittle failure (Fig. 7). The ascending pulses of seismicity-enabling fluid, being CO_2-poor, certainly do not represent new mantle-derived inputs and are most likely released intracrustally from the crystallizing rhyolitic residue.

The upper limit of abundant SMSZ seismicity at ~3 km depth (Fig. 5 of Prejean et al., 2002) could represent a hydrothermally sealed lid, which at ~12 km long (east-west) would be a surprising regularity; or it may simply reflect upward dissipation of pressure as fluid pulses spread laterally during ascent through the fracture network in the ring-fault zone. At 3 km depths, SMSZ earthquakes are in basement rocks of the downfaulted roof plate and in their shattered equivalent in the step-faulted ring-fault zone. A few earthquakes scatter to depths as shallow as ~2 km, where they are close to the local base of the intracaldera Bishop Tuff (Figs. 7, 8).

The model of fluid-driven uplift requires that the updomed cauldron block (roof plate), most of which is aseismic, low in temperature, and devoid of fluid emissions, should be relatively impermeable, ductile at depth, and thick. Because most of the confining ring-fault zone is also aseismic and emission-free, it is inferred to be sealed and thus likewise impermeable, leaving ascending fluid no egress save the 12-km-long segment along the SMSZ. At Campi Flegrei caldera (Italia), Vanorio and Kanitpanyacharoen (2015) showed that core samples of the updomed caprock that confines the seismogenic hydrothermal system consists of fine-grained tuff that has been altered to a dense calc-silicate mineral assemblage with a fibrous structure that enhances its shear and tensile strength. Recrystallization of the kilometer-thick tuff layer has created a lid that is impermeable enough to confine overpressured fluid but ductile enough to accommodate the bending strain as fluid pressure increases while resisting fracture.

Similarly at Long Valley caldera, scrutiny of the 3-km-deep LVEW core by McConnell et al. (1995, 1997) showed most components of the roof plate to be of low permeability. The Bishop Tuff is densely welded, devitrified, contains chlorite, pyrite, and pervasive calcite, with a dense groundmass mosaic of secondary quartz, clay minerals, and calcite. Intruding the Bishop Tuff are 10 sills of fine-grained aphanitic Early Rhyolite, the stack of which (Fig. 8) would alone provide an impermeable barrier. The thickest of the sills are 106, 43, 40, and 17 m thick, and their cumulative thickness is 330 m. They are densely microcrystalline and argillized, containing illite, mixed-layer illite-smectite, and pervasive calcite and secondary quartz. The basement rocks include chlorite- and epidote-bearing metavolcanic rocks but are predominantly fine-grained laminated silicic and pelitic hornfels with subordinate quartzite and marble interbeds. Fractures are filled with quartz, calcite, pyrite, chlorite, epidote, and pervasive clay minerals. Most lithologies in the aseismic cauldron block are thus fine-grained, non-granitic, dense, and dry. As illustrated in Fig. 7, low permeability of a thick roof plate is consistent with diversion of the pressurizing fluid toward the SMSZ from depths of 7–9 km.

9. Structure of the Pleistocene resurgent uplift

At least 400 m uplift of the resurgent dome was largely accomplished before 570 ka. No radial or concentric faults, as might be associated with domical uplift, are present. The fault system cutting the dome is dominated by NNW trends (Fig. 1), roughly parallel to those of rangefront faults north and south of the caldera and also parallel to the strike of steeply dipping structures and bedding in metamorphic basement rocks that make up most of the subsided caldera floor. The two grabens, Fumarole Valley and Smokey Bear Flat, are neither *medial* nor *apical* (as often recited) but, instead, transect flanks of the uplifted region. The pattern of faults on the uplift is more congruous with Basin and Range extension than with the radially symmetrical ongoing inflation.

Although the resurgent dome is roughly circular in plan view and 10 km wide, it is structurally complex, but none of the dome-crossing faults are observed to have been reactivated by the 83-cm recent uplift, which is also nearly circular in plan (Montgomery-Brown et al., 2015). The Pleistocene resurgent structure, however, is more like the opposing pair of bulkhead doors on a NNW-elongate storm cellar. Grossly, the opposing limbs dip WSW and ENE, with multi-block complexity along both downset grabens. The total uplift since 1980 amounts to ~0.2% (0.002) of the middle Pleistocene resurgent uplift. Unrest and resurgence are not the same.

9.1. Area of the current uplift

Since 1980, the cumulative uplift of ~83 cm has taken place in several episodes and was measured by a sequence of levelling, trilateration, EDM, GPS, and InSAR (Hill, 2006). Attention has been concentrated on the Pleistocene resurgent dome, an area 10 km in diameter, near the south-center of which the uplift has been greatest (Savage et al., 1987; Langbein, 2003; Montgomery-Brown et al., 2015). The Pleistocene

resurgent uplift, as inferred from tilted strata and drillhole data, is confined inside the ring-fault zone and is probably bounded closely by it on its north and south sides (Figs. 1, 2).

The original levelling studies, however, described a roughly symmetrical area of domical upwarping >30 km in diameter that extends far beyond the Pleistocene uplift and even well outside the caldera. Along Highway 395, 5–10 cm of the uplift extends as far northwest as June Lake Junction (10 km outside the caldera) and as far southeast as the Hilton Creek fault (~2 km outside the buried structural boundary of the caldera) (Fig. 4 of Savage and Lisowski, 1984; Figs. 7–10 of Savage et al., 1987). Rather than just bending the caldera's roof plate, the deformation impacts a region well outside the ring faults. If the regional tectonic stressfield is important in driving the uplift, why is the ongoing uplift radially symmetrical? On the other hand, if uplift broader than the caldera itself were caused by subcaldera processes alone, why are there no earthquakes along most of the ring-fault zone? Must one not infer that the ring-fault zone remains stably sealed everywhere except along its short south-moat segment (Figs. 3, 4) where it has been reactivated adjacent to the seismically dynamic Sierran block?

The contrast between broad pan-caldera, radially symmetrical doming and the localized SMSZ seismicity is hard to reconcile with the idea of recent intrusion of a dike, which in this structural setting could be expected to be oriented NNW. Moreover, the episodic pulses of uplift may be more compatible with sporadic ascent of distributed pore fluid than with staccato advance of a rapidly freezing dike.

10. Resurgent dome: normal heat flow and low seismicity

Nearly all deep drillholes on or around the Pleistocene resurgent structure have thermal profiles that show reversals with depth, near-normal geothermal gradients below the reversals, and/or large isothermal segments at their bottoms (Sorey et al., 1991; Farrar et al., 2003; Hurwitz et al., 2010). Well LVEW, centered on the resurgent uplift, displays a constant temperature of ~100 °C from a depth of 2000 m to its bottom at nearly 3000 m. At the Casa Diablo geothermal plant, Well M-1 showed a sharp reversal beneath the geothermal aquifer, thus yielding a temperature of only ~100 °C at its 1605-m total depth. Well CP at the eastern foot of the resurgent area had a bottom-hole temperature of 148 °C at a depth of 1847 m. Well 13–26 at the southeastern foot of the resurgent area had a bottom-hole temperature of 110 °C at a depth of 1186 m, and Well 13–21 just north of Fumarole Valley had 99 °C at 1111 m. Three more wells on the west wall of Fumarole Valley have bottom-hole temperatures of 123–129 °C at depths of 327–607 m; and their fluids were inferred by Hurwitz et al. (2010) to reflect shallow lateral hydrothermal flow eastward along the southern fringe of the resurgent uplift, from the caldera's west moat *via* Casa Diablo. They concluded that the modest temperatures, the deep isothermal segments, and the contrast of the warm seismic southern fringe of the resurgent structure with its cold aseismic major part are not consistent with the presence of upper-crustal magma beneath it.

Before the drilling of LVEW demonstrated 100 °C isothermal conditions at 2–3 km depths, the rarity of earthquakes beneath most of the resurgent structure had been interpreted to suggest that the brittle-ductile transition is as shallow as 5 km beneath the uplift (Hill, 1992), whereas seismicity close nearby extends to depths of 10 km beneath the SMSZ and to 15 km in the adjacent Sierra. Because the seismogenic domain of the SMSZ extends northward beneath a 2.5-km-wide southern fringe of the resurgent dome (Fig. 4), where abundant brittle-failure earthquakes are as deep as 9–10 km (Fig. 5 of Prejean et al., 2002), I am skeptical that the brittle-ductile transition could rise steeply to only ~5 km depth within only another kilometer or so northward under the main aseismic part of the cold Pleistocene dome where the current uplift is centered. Moreover, as the transition is typically identified in crustal rocks around 400 °C, for ductility to set in at a depth of 5 km would require a gradient of ~150 °C/km directly beneath the contiguous 100 °C isothermal segment at 3 km.

Alternatively, because there is neither any seismicity at any depth beneath most of the uplift nor beneath most of the circumcaldera ring-fault zone, the brittle-ductile transition may be ~10 km deep (as in the south moat). Aseismicity of the uplift suggests that fluid ascent from the dying rhyolitic pluton pressurizes the resurgent flexure at a depth near 10 km, thence escapes laterally to the SMSZ (Fig. 7). Only along a 12-km-long, 10-km-deep segment of the ring-fault zone in the south moat, contiguous with the seismically dynamic Sierran block, are caldera earthquakes manifest (Fig. 4).

In advocating and defending a model of magmatic intrusion at depths of 6–8 km to account for the ~83 cm of uplift since 1980, proponents appeal to the slow rate of thermal conduction to explain the absence of any tell-tale thermal signal at a depth of 3 km. At some depth greater than the isothermal lower reach of the 3-km-deep LVEW corehole, a positive geothermal gradient must resume. The argument that purely conductive heat flow has not yet had time to manifest the thermal signal of an intrusion at 6–7 km depth seems tenuous for an area intimately semi-encircled by a fringe of manifestly vigorous convective heat flow and fluid-mediated seismicity as deep as 10 km. Heat transport around the south edge of the area of ongoing uplift is not confined to the eastward-flowing shallow geothermal aquifer but is augmented by fluids ascending beneath it from depths at least as great as 9–10 km (Prejean et al., 2002; Shelly et al., 2016).

Some thought to explain the 100 °C temperatures at 2–3 km depth by invoking downflow of cold meteoric water. Investigation of temperature, fluid flow, and geoelectrical data for LVEW by Pribnow et al. (2003), however, ruled out such downflow. They calculated that convective heat transport dominates the resurgent dome at LVEW, being 1–4 times more effective than heat conduction, and they inferred that the low thermal gradient is related to upflow of cool formation fluids from Paleozoic rocks of the roof plate. Hydrothermal mineral deposits in Well LVEW and at springs around the resurgent dome suggest that high-temperature fluid-circulation (250°–350 °C) waned after ~300 ka (Sorey et al., 1991; McConnell et al., 1997; Fischer et al., 2003). A quarter-million years of hydrothermal cooling has lowered the temperature by ~200 °C in LVEW and probably by comparable amounts to depths as great as 10 km beneath the aseismic resurgent dome.

Aseismicity is incompatible with ongoing intrusion beneath the area of uplift. In contrast, under Mammoth Mountain, where CO_2 and He emissions provide good evidence of gas release from mantle-derived basalt, seismicity is abundant from the near-surface to depths as great as 30 km (Shelly and Hill, 2011; Dawson et al., 2016).

11. Absence of CO_2 flux beneath the area of ongoing uplift

Following a 1989 earthquake swarm under Mammoth Mountain, onset of tree-killing magmatic CO_2 emissions took place within 5–16 months (Cook et al., 2001). A deep swarm below Mammoth Mountain in 2009 was followed within one year by a doubling of CO_2 emissions at the Horseshoe Lake tree-kill area (Lewicki et al., 2014). Werner et al. (2014) pointed out that yet another pulse of CO_2 emissions had taken place in 2000–2001, subsequent to Mammoth Mountain seismicity that had peaked in November 1997, so within ~3 years. Total CO_2 emission at Mammoth Mountain was estimated to be 1200–1300 tonnes/day (t/d) in the early 1990s (Farrar et al., 1995); 250 t/d in 1998 (Gerlach et al., 1999); 416 t/d in 2011 (Werner et al., 2014); and 311 t/d in 2013 (Lewicki et al., 2014). In contrast, total CO_2 emissions for 13 tree-kill and bare-ground sites along the hydrothermally active south-flank fringe of the resurgent uplift was merely 8.7 t/d in 2003–2004 (Bergfeld et al., 2006). These authors concluded (a) that so weak a flux of CO_2 was easily provided by the shallow geothermal aquifer (sourced in the west moat), (b) that there is virtually no CO_2 emission along the south moat proper or from the main part of the resurgent uplift, and (c) that there is no evidence for input of magma or magmatic fluids beneath the caldera. Moreover, a carbon-isotope study of soil gas (Lucic et al., 2015) showed that the sparse soil CO_2 overlying the

geothermal aquifer has a modest magmatic-hydrothermal contribution (transported from the west moat) but that the sparse soil CO_2 elsewhere along the south moat, on the caldera floor, and on the main resurgent uplift is predominantly biogenic.

If CO_2 emission responds to seismic swarms under Mammoth Mountain within 1–3 years, why has there been no emission of magmatic CO_2 on the resurgent structure in the 37 years since measured uplift started in 1980—if the uplift were indeed promoted by upper-crustal intrusion of CO_2-rich mafic magma? There are numerous faults across and around the resurgent dome and steeply dipping bedding in the subsided roof plate beneath it that could have facilitated ascent of CO_2—had it actually been released into the subcaldera crust. The lack of CO_2 emission essentially precludes mantle-derived mafic (or intermediate) magma as a pressure source for the ongoing uplift.

The absence of CO_2 ascent beneath the uplift and most of the caldera apparently precludes a still-active subcaldera mantle like those inferred to provide vigorous CO_2 fluxes at Yellowstone and Campi Flegrei calderas and, neaby, beneath Mammoth Mountain and the west moat. It further supports the inference that the seismicity-facilitating fluid flux at Long Valley is low-viscosity aqueous fluid from intracrustal crystallization of the long-lived subcaldera rhyolitic/granitic pluton.

12. Helium isotope ratios

Suemnicht et al. (2015) reported abundant He-isotope data for fumaroles, hot springs, and geothermal fluids across the caldera. They noted the absence of high-temperature fumaroles, absence of elevated CO_2, SO_2, and halogens, and general lack of magmatic signatures in Long Valley fluids. $^3He/^4He$ values around the resurgent dome are only 2.7–4.9 R_A. Farther east at Hot Creek and Little Hot Creek, values in the range 4.5–6.1 were reported, and the authors suggested that the higher values distal to the hydrothermal aquifer might reflect modest additions of mantle-derived gas that rise along strands of the buried (precaldera) Hilton Creek fault zone (Fig. 4). For central and southern parts of the caldera, however, including the SMSZ and the resurgent structure, they concluded that low heat flow and negligible magmatic signatures in the fluids weigh strongly against any new injection of magma into the crust. From the fluid data, Suemnicht et al. (2015) also inferred low permeability for the caldera roof plate, thus reinforcing my conclusion (Section 8, above) that the fluid-pressurized domain is capped by a low-permeability lid ~5–7 km thick (Fig. 7), which is ductile enough to permit recurrent updoming and impermeable enough to require the fluid to escape laterally to the tectonically reactivated fracture network of the south-moat ring-fault zone.

At Mammoth Mountain, the association of seismic swarms, mid-crustal long-period earthquakes, brittle-failure earthquakes as deep as 30 km, elevated CO_2 emissions, and episodes during which $^3He/^4He$ has risen to values as high as 6.7 R_A implicates intracrustal ascent and degassing of mantle-derived basalt (Sorey et al., 1993; Shelly and Hill, 2011). The lack of such associations accompanying the SMSZ swarms and lack of any such signals at all beneath the old cold resurgent dome is further evidence against recent subcaldera ascent of basalt.

No magmatic gas, modest heat flow, and no seismicity compels the inference that there is no new magma beneath the area of uplift. Not all bulges are what they appear to be. If not a new intrusion, the most plausible and compelling alternative physical model is aqueous fluid being released by late-stage solidification and second boiling of Long Valley's formerly capacious rhyolite reservoir.

13. Published models of pressure sources for uplift

A wide variety of source models have previously been proposed to account for the recent deformation at Long Valley, nearly all assuming magmatic intrusion beneath the resurgent dome. Geodetic models have included plutons, sills, point sources, spherical bodies, and prolate ellipsoids—pipelike or squat, single or paired, vertical or inclined, deep or shallow, and with or without a viscoelastic shell.

Deformation data through 1985 were modeled as the product of two Mogi point sources of inflation at depths of 5 and 10 km beneath the resurgent dome, spaced ~5 km apart laterally, along with dextral slip in the south moat (Langbein et al., 1987; Langbein, 1989). Renewed uplift in 1989–1991 was attributed to a single Mogi point source centered beneath the resurgent dome at 6–8 km depth, with little contribution from other sources; and the revised model was said to account for most of the deformation accumulated since 1979 (Langbein et al., 1993). Completion of a new levelling survey in 1992 and its combination with extensive trilateration data led to yet a new model that replaced spherical point source models with a pair of prolate ellipsoidal sources—one as shallow as 5.5 km beneath the resurgent dome and another (less well defined) said to plunge NE at 10–20 km beneath the south moat (Langbein et al., 1995). Renewed uplift in 1997–1999 led Langbein (2003) to further modifications—a near-vertical prolate spheroid as the principal pressure source under the resurgent dome at 6–7 km depth, dextral slip in the south moat, and a mid-crustal inflation source at 12–20 km beneath the south moat. Analysis of InSAR data, however, led Thatcher and Massonnet (1997) and Fialko et al. (2001) to model only a single pressure source (under the resurgent dome); the latter study favored a prolate spheroid at a depth of 7.2 km. Using the EDM and levelling data for the 1988–1992 interval, on the other hand, Tiampo et al. (2000) compared spherical Mogi and prolate spheroidal models for two inferred pressure sources—a larger one at 9–10 km beneath the resurgent dome and a lesser one at 7–12 km beneath the south moat. Battaglia et al. (2003a) combined GPS data with levelling and EDM measurements to model a pressure source beneath the resurgent dome as a vertically elongate prolate spheroid with an aspect ratio somewhere between 0.25 and 0.65, at a depth somewhere between 4.9 and 7.5 km, and representing a volume change between 0.06 and 0.13 km^3. Clearly, none of these models is unique.

Nearly all the models assumed the upper crust to behave as a homogeneous, isotropic, purely elastic solid, which it obviously is not. The 2–3 km of caldera fill consists of subhorizontally disposed strata, broadly arched and faulted by middle Pleistocene resurgence, that range in density from lake silt, beach gravel, and glacial till to variably welded tuff, rhyolite, and basalt. In contrast, the subsided roof plate beneath the fill consists of subvertical Paleozoic metasedimentary strata intruded locally by subordinate bodies of Mesozoic granodiorite. The steeply dipping strata probably also underlie the crystalline and partially molten residues that remain of the Bishop Tuff and Early Rhyolite magma body. If a recent upper-crustal intrusion were really the pressure source for intracaldera uplift, its shape would probably be influenced by the host-rock layering, whether horizontal, vertical, or otherwise. If emplaced within the steeply dipping basement strata of the roof plate at 2–8 km depths, such a conjectured intrusion could be expected to be steeply tabular and to strike NNW.

Newman et al. (2006) did not consider the host-rock structure, but they avoided the elastic approximation by modeling a vertical prolate spheroid at 6 km depth encased within a viscoelastic shell 0.5–1 km thick. This, they argued, would increase the effective volume of the pressure source, would lower the pressure needed for a given surface deformation, and would sustain uplift well after the peak pressure episode. They were thinking in terms of a magmatic intrusion, but their scenario seems equally applicable to ascending pulses of slowly dispersing near-solidus granite-derived aqueous pore fluid.

13.1. Gravity models

Source models that combine microgravity data for Long Valley with the varied geodetic measurements were pioneered by Battaglia et al. (1999). For the interval 1982–1998, they measured decreases in gravity throughout the caldera that were as great as -107 ± 6 μGal over the resurgent dome. After correcting for uplift and loosely estimated water-

table fluctuations, residual gravity changes were calculated to be positive at several stations and as great as +64 ± 15 μGal locally on the resurgent dome. Assuming a point-source intrusion, they estimated its depth to be 10.0–13.8 km, its mass increase to be 7.4×10^{11} kg, and its volume increase to be 0.16–0.32 km^3, from which they judged density of the intrusion to be in the range 2700–4100 kg/m^3, leading them to infer it to be basaltic. This is inconsistent with lack of CO_2 and He signals, as discussed above.

Accumulating geodetic data and an expanded microgravity survey in 1999 led Battaglia et al. (2003a, 2003b) to revise their model. They next proposed a vertically prolate spheroidal intrusion with an aspect ratio of 0.475 at a depth of 4.9–7.5 km under the resurgent dome, where its volume change was estimated to be 0.105–0.187 km^3 and its density in the range 1180–2330 kg/m^3 (half the previous density estimate), leading them to infer a hybrid magma-plus-fluid intrusive mass. Using much the same data, Battaglia and Vasco (2006) explored a more general 3-dimensional distribution of inflation, estimating fractional volume changes in ~5000 grid blocks beneath the resurgent dome. This exercise calculated a principal inflation volume at 5–7 km depth, elongate west–to–east, extending for 10 km beneath the southern third of the resurgent dome. A secondary inflation volume, 2.5 by 3.5 km across but likewise 5–7 km deep, was modeled beneath Gilbert Peak, centered ~6 km north of the first.

Using the same 1982–1999 microgravity data, Tizzani et al. (2009) added 1992–2000 InSAR imagery and EDM data for many baselines to propose a revised model of the postulated intrusive source, the geometry of which they assumed had not changed over the two decades concerned. They then modeled a prolate spheroid with an aspect ratio of 0.56–0.84 that plunges 30°–77°SW at a depth of 6.6–8.7 km, and they recalculated its density to lie in the range 2192–3564 kg/m^3 (back to basalt?). The volume change was said to be 0.682 km^3, which is 4–7 times greater than the earlier estimates that used the same gravity data.

This summary should make obvious that the gravity inversions are far from unique and that estimates of depth, volume, density, and shape of any inferred intrusive source are highly uncertain and overinterpreted. Scrutiny of the residual gravity pattern (Fig. 4B of Tizzani et al., 2009) reveals extremely erratic distribution. The peak amplitude of the changes in residual gravity (on the east side of the resurgent dome), 66 ± 11 μGal, is matched by values of 64 ± 20 μGal well outside the resurgent dome to the northwest and 63 ± 33 μGal in the lowland moat near the airport. Another outboard station, on undeformed lakebeds northeast of the Hot Creek flow, gives 52 ± 22 μGal, one of several positive residual gravity change where there is no uplift. Moreover, within the western half of the uplifted area, one station actually shows a decrease in residual gravity at −3 ± 22 μGal. The erratic gravity pattern may reflect large uncertainties in water-table variations, in statistical interpolation of free-air corrections, and in porosity and density variations in lithologically complex sections underlying the gravity stations. In any case, the adjusted residual data (Fig. 4B of Tizzani et al., 2009) were severely cherry-picked to arrive at the model advanced.

Contrary to the assertion by Tizzani et al. (2009) that magma is "unambiguously" the cause of Long Valley unrest, the weakness of the gravity models shows that the material nature of the inflation source and the very existence of an intrusive body remain unproven.

13.2. Disparity between modeled pressure source and its volume increase

A recent comprehensive model of the location and dimensions of the inflation source (Montgomery-Brown et al., 2015) appears to fit all the relevant geodetic data. They modeled inflation of a near-vertical prolate ellipsoid with its centroid at a depth of 7.2 km, a major radius of 3.05 km, and minor radii of 1.73 km, dimensions that yield a volume of 38.24 km^3 (Fig. 7). Within the ellipsoid, they estimated the volume change that promoted the 2011–2014 inflation episode to be 6.9×10^6 m^3 per year (or ~22.8×10^6 m^3 for the 3.3-year interval considered). The model thus suggests that the material introduced (or expanding in place) occupied only 0.06% of the ellipsoid volume. Similar, if less extreme, mismatches attend previously published estimates of pressure sources for uplift since 1980. A revised version of the model by Hill and Montgomery-Brown (2015) gives a cumulative increase since 1980 in ellipsoidal source volume of 1.2%.

Their analysis suggests that the centroid and the ellipsoid as a whole has been stationary, showing no evidence of ascent during the decades of geodetic measurements and modeling. The radial symmetry of the ongoing uplift is thought to be inconsistent with intrusion of a tabular dike or sill. The modeled ellipsoid may never have been an ascending body at all, but, instead, a porous or fractured domain suffused with fluid ascending from the crystallizing Pleistocene pluton below. Expansion of a distributed mobile interstitial phase would pressurize the ellipsoid from within. The very small volume fraction within a 38-km^3 inflating domain modeled (Fig. 7) is more consistent with introduction and poroelastic expansion of low-viscosity fluid—either interstitial or within a distributed fracture network—than with a tiny fraction of interstitial rhyolitic melt. The most reasonable geologic agent is low-CO_2 aqueous fluid expelled from ultimate crystallization of the granitic residue of the formerly great Long Valley rhyolitic reservoir, by second boiling.

14. Seismicity and structures in the adjacent Sierran block

The Hilton Creek fault (Fig. 4) strikes N20°W along the east side of the seismically active Sierran block, which forms the south wall of the caldera. The down-to-the-east normal fault, inferred to have been active since early Quaternary time, controls a great scarp with ~1100 m relief that provides an eastern free face for the Sierran block. Although it produced ~17 m of postglacial normal displacement on MIS-2 moraines at McGee Creek, the Hilton Creek fault has not been seismically active during any of the 1978–2017 earthquake episodes nearby. Within the Sierran block, several belts of diffuse seismicity have been recurrently active, and high-resolution relocations condensed these belts into four (or five) discrete cryptic fault zones within the block (Prejean et al., 2002; Hill et al., 2002; Hill, 2006). Two of them virtually impinge on the Hilton Creek fault obliquely, and a third (SNB4 of Prejean et al., 2002) crosscuts and terminates the reach of the beheaded Hilton Creek fault that remained active in postcaldera time south of the caldera. Although the Hilton Creek fault is commonly depicted as continuing into the caldera, there is no evidence of postcaldera slip north of its apparent truncation by the cryptic fault SNB4 (Fig. 6 of Prejean et al., 2002).

Several of the cryptic faults in the south moat share with extracaldera SNB4 dextral focal-plane solutions, WNW strikes, and steep NNE dips (Table 2 of Prejean et al., 2002). Moreover, only a 3-km-wide gap, covered by till and alluvium, separates SNB4 from the apparent end of the great Round Valley fault, which also locally strikes WNW and has a large dextral component to its major transtensional displacement (Hildreth and Fierstein, 2016b; Phillips and Majkowski, 2011). That the dextral component is currently being extended from the Round Valley fault into the caldera's south moat is further evidence of the intracaldera dominance of regional tectonic stress.

The SMSZ, along which dextral focal-plane solutions predominate (Prejean et al., 2002), has been called a "leaky transform fault" by Hill and Montgomery-Brown (2015). However, there have been no "leaks" (eruptions) along the south moat since the Hot Creek flow at 333 ka. Moreover, although the ring-fault zone has been there since 767 ka, no surface displacements are recognized. The south moat is floored by several mafic lava flows, all of which yield $^{40}Ar/^{39}Ar$ ages between 180 and 92 ka (Hildreth et al., 2014), but none of them is faulted, dextrally or otherwise, within the SMSZ (Hildreth and Fierstein, 2016a). The cryptic dextral faulting modeled by Prejean et al. (2002) may be of very recent origin, perhaps as young as 1980.

None of the cryptic faults, in either the Sierra or the caldera, is known to have surface expression, so all could be of relatively recent origin. How can the dominant seismicity in the area, including at least 12 events of *M*5.0–*M*6.1 (Prejean et al., 2002), located only 0 km to 8 km west of the Hilton Creek fault, have taken place without activating that great free-standing block-bounding fault itself? Why should the ENE-WSW extension inferred locally (Fig. 10 of Prejean et al., 2002; Hill et al., 2002) induce apparent sinistral slip within the Sierran block and complementary dextral slip in the SMSZ, without reactivating normal slip on the adjacent Hilton Creek fault?

Four belts of seismicity relocated as cryptic fault zones in the Sierran block by Prejean et al. (2002), have the following orientations: (a) 359° @ 64°E, 12-km long and forming the western boundary of abundant Sierran seismicity; (b) 21° vertical, 9 km long, sinistral; (c) 26° vertical, 5.6 km long, sinistral; and (d) 298° @ 60°NE, 5 km long, dextral. These seismic belts crosscut at high angles the structure of the Mount Morrison pendant, in which the Paleozoic strata strike roughly 330° and are typically disposed near the vertical (dipping 50°–90°; Rinehart and Ross, 1964; Greene and Stevens, 2002). The cryptic Sierran seismicity extends from near the surface to depths of 12–15 km (deeper than the 9–10 km in the SMSZ), depths at which the pendant strata may (or may not) be rooted in more massive plutonic rocks. Nonetheless, is it not remarkable that the several arrays of Sierran-block earthquakes are completely unaffected by the NNW regional trend of the steeply dipping basement strata? Or by the NNW trend of the main rangefront faults near Long Valley?

If seismicity in the Sierran block is directly implicated in activating seismicity along the south moat ring-fault zone, as advocated here, and if that ring-fault fracture network provides the main escape path for granite-derived aqueous fluid ascending beneath the ongoing uplift (Fig. 7), then we need to learn more about the stressfield and neotectonics of the adjacent Sierra Nevada.

15. Summary and conclusions

Since nearly continuous seismicity started in the Sierran block next to Long Valley in 1978–1980, intracaldera unrest has included (1) episodes of uplift centered on the middle Pleistocene resurgent dome and (2) recurrent seismic swarms in a 12-km-long segment of the ring-fault zone along the caldera's south moat. This South Moat Seismic Zone follows the southern fringe of the otherwise aseismic inflating domain and is continuous with the extracaldera seismogenic domain in the Sierra Nevada. Geodetic data indicate ~83 cm of uplift since 1980 and define a radially symmetrical area of inflation coincident with the postcaldera vent cluster for the Early Rhyolite (750–640 ka) and with the area subsequently uplifted as a 10-km-wide resurgent dome (Fig. 1). Uplift was largely accomplished by 570 ka, but smaller increments took place later.

The shallow rhyolitic magma body that fed the 100 km^3 of Early Rhyolite, and last erupted in mid-caldera ~330 ka, should by now, with no apparent basaltic thermal sustenance, have reached an advanced stage of crystallization, solidifying into a granitic pluton. Although at least 20 tomographic experiments were undertaken, no magma body has ever been convincingly imaged.

A caldera-wide low-velocity domain at 8–14 km depth advocated by Seccia et al. (2011) just might be the plutonic residue and its superjacent fluid halo. The pressure source for ongoing uplift, however, has been attributed by most geodeticists and seismologists to ascent of a new magmatic intrusion. Geologic evidence weighs against a new intrusion for the following reasons.

1. There was a 100-fold drop in volumetric eruption rate in the caldera after 640 ka, and there has been not a single eruption on the fault-laced resurgent dome in 500,000 years.
2. Focussed clusters of volcanic vents mark a series of eruptive episodes that progressed southwestward from Glass Mountain to Mammoth Mountain systematically for 2 Myr (Fig. 2). It would be unprecedented for a new intrusion to backtrack to the mid-caldera today.
3. There have been no mafic eruptions anywhere near the main part of the caldera to its north, south, or east since the Pliocene, nor have there been any mafic enclaves in intracaldera lavas, which are exclusively rhyolitic, since 500 ka. The mantle has been unproductive beneath most of Long Valley caldera and its periphery, allowing the main rhyolitic reservoir to approach solidification since its last small Moat Rhyolite extrusions ~330 ka.

The multi-vent basalt-to-dacite Mammoth magmatic system (230 ka to the present), southwest and west of the structural caldera, has provided thermal support for reactivation or survival of Long Valley rhyolitic crystal mush in the contiguous west moat, but only in the west moat, far from the resurgent dome.

4. Hydrothermal mineral deposits in Well LVEW and at springs around the resurgent dome suggest that high-temperature fluid-circulation (250–350 °C) waned after ~300 ka (Sorey et al., 1991; McConnell et al., 1997; Fischer et al., 2003).
5. Beneath the Pleistocene resurgent dome, there is almost no seismicity at any depth, no evidence for active contributions of mantle-derived He, no emission of magmatic CO_2 or any other magmatic gases, and normal to below-normal heat flow. Well LVEW, centered atop the resurgent dome, is isothermal at 100 °C from a depth of 2 km to its bottom at 3 km, even though it had hosted hydrothermal circulation at 300° ± 50 °C as late as 300 ka.
6. SMSZ seismicity is not driven by stress associated with the nearby uplift, which would impede the dextral slip inferred there (Prejean et al., 2002). Rather, it is driven by regional tectonic stress (Hill, 2006), and its dextral component is collinear with longstanding dextral slip along the nearby segment of the Round Valley rangefront fault.
7. Compared to the SMSZ, the contiguous Sierran seismogenic domain had 1.6 times as many *M*3 (or greater) earthquakes and 3.6 times the cumulative seismic moment from 1980 to 2015. The major seismicity that began in the Sierra in 1978–1980 apparently triggered activation of the adjacent ring-fault zone along the south moat. The ring-fault zone has been there since 767 ka, but only the 12-km-long segment (Figs. 3, 4) directly contiguous with the Sierran seismogenic domain has been seismically active since 1980. The resurgent dome and 300° of the 75-km-long ring-fault circumference are seismically quiescent, even though the ongoing uplift is centered within it.
8. At the Mammoth basalt-to-dacite volcanic field just outside the structural caldera, basalt erupted as recently as 8000 years ago, abundant seismicity extends from the near-surface to depths of 30 km, spikes in He-isotope ratio are as high as 6.7 Ra, and copious CO_2 discharge is widespread and persistent since 1990. Few would question the existence of a magmatically active mantle and deep crustal intrusion of derivative basalt beneath the Mammoth system. Pulses of increased CO_2 emission follow seismic swarms at Mammoth Mountain within 1–3 years. In central Long Valley caldera, on the contrary, 37 years of seismicity has prompted no local CO_2 emission at all. And thermal, seismic, He, and CO_2 signals of intrusion are absent beneath the Pleistocene resurgent dome, which is the center of recent uplift.
9. Detailed analysis of a months-long earthquake swarm in 2014 at the southeast toe of the resurgent dome resolved numerous episodes of upward-migrating seismic activity within a network of cryptic faults (Shelly et al., 2016). An expanding fluid-pressure pulse triggered activity on a family of neighboring faults, and the upward migration of hypocenters in several weeks-long episodes was interpreted to be promoted by rapid ascent of high-pressure low-viscosity aqueous fluid (Shelly et al., 2016). Entering the brittle crust from deeper than 8 km, such fluid is just what would be predicted for ascent

from the rhyolitic pluton undergoing late-stage crystallization and second boiling at 8–14 km depth (Fig. 7). The absence of CO_2 and ^3He signals is consistent with fluid from a (non-mafic) rhyolitic source, and upward decay of more diffuse seismicity is what might be expected of pressurized fluid that first promotes centered uplift and then escapes laterally in pulses into the SMSZ ring-fault network.

It is concluded that degassing of the crystallizing residue of the pluton-scale subcaldera rhyolitic magma body releases low-CO_2 aqueous fluid that ascends and pressurizes a hydrothermal system beneath the resurgent dome, a structural flexure older than 570 kyr. Increments of fluid release and resulting pulses of additional updoming have probably been intermittent throughout much of the late Pleistocene, with the recent deformation simply being the latest episode. No magma ascent is required. Crystallization-induced volatile exsolution leads to aqueous fluid escape, which in turn enhances further crystallization of the moribund rhyolitic reservoir in its ultimate transformation into a leucogranite pluton. The fluid-pressurized domain is capped by a low-permeability lid ~5–7 km thick (Fig. 7), which is ductile enough to permit recurrent updoming and impermeable enough to require the fluid to escape laterally to the tectonically reactivated fracture network of the south-moat ring-fault zone. The fluid source dates from the middle Pleistocene, the perturbation from 1980.

Acknowledgments

I am grateful to Emily Montgomery-Brown, Bernard Chouet, Phil Dawson, Bill Ellsworth, Shaul Hurwitz, Mitch Pitt, Stephanie Prejean, and especially Dave Hill for helping me grapple with the geophysical puzzles. None should be inferred to have fully accepted all my arguments. The meticulous studies by Stephanie Prejean and Dave Shelly have been fundamental to our current understanding of Long Valley unrest. Field geologists always benefit from the work of those who have gone before. At Long Valley, admirable contributions have been made by Roy Bailey, Deb Bergfeld, John Eichelberger, Bill Evans, Chris Farrar, Judy Fierstein, Jim Howle, King Huber, Steve Lipshie, Gail Mahood, Larry Mastin, Vicki McConnell, Jenny Metz, Dan Miller, Bill Putnam, Dean Rinehart, Don Ross, Mike Sorey, Gene Suemnicht, and Colin Wilson. Manuscript reviews by Bernard Chouet, Shaul Hurwitz, John Stix, and Gene Suemnicht are deeply appreciated.

References

Bailey, R.A., 1978. Volcanism, Structure, and Petrology of Long Valley Caldera, California. (PhD dissertation). The Johns Hopkins University, Baltimore, Maryland (112 p).
Bailey, R.A., 1989. Geologic map of Long Valley caldera, Mono-Inyo Craters volcanic chain, and vicinity, eastern California. U.S. Geological Survey Map I-1933 (scale 1:62,500, 2 sheets; pamphlet 11 p).
Battaglia, M., Vasco, D.W., 2006. The search for magma reservoirs in Long Valley Caldera: single versus distributed sources. In: Troise, C., DeNatale, G., Kilburn, C.R.J. (Eds.), 2006, Mechanisms of Activity and Unrest at Large Calderas. 269. Geological Society of London, pp. 173–180 (Special Publication).
Battaglia, M., Roberts, C., Segall, P., 1999. Magma intrusion beneath Long Valley Caldera confirmed by temporal changes in gravity. Science 285 (p. 2119–2112).
Battaglia, M., Segall, P., Murray, J., Cervelli, P., Langbein, J., 2003a. The mechanics of unrest at Long Valley caldera, California: 1. Modeling the geometry of the source using GPS, leveling and two-color EDM data. J. Volcanol. Geotherm. Res. 127, 195–217.
Battaglia, M., Segall, P., Roberts, C., 2003b. The mechanics of unrest at Long Valley caldera, California: 2. Constraining the nature of the source using geodetic and micro-gravity data. J. Volcanol. Geotherm. Res. 127, 219–245.
Bergfeld, D., Evans, W.C., Howle, J.F., Farrar, C.D., 2006. Carbon dioxide emissions from vegetation-kill zones around the resurgent dome of Long Valley caldera, eastern California, USA. J. Volcanol. Geotherm. Res. 152, 140–156.
Black, R.A., Deemer, S.J., Smithson, S.B., 1991. Seismic reflection studies in Long Valley caldera, California. J. Geophys. Res. 96, 4289–4300.
Candela, P.A., 1997. A review of shallow, ore-related granites: textures, volatiles, and ore metals. J. Petrol. 38, 1619–1633.
Candela, P.A., Blevin, P.L., 1995. Do some miarolitic granites preserve evidence of magmatic volatile phase permeability? Econ. Geol. 90, 2310–2316.
Chiodini, G., Vandemeulebrouck, J., Caliro, S., D'Auria, L., DeMartino, P., Mangiacapra, A., Petrillo, Z., 2015. Evidence of thermal-driven processes triggering the 2005–2014 unrest at Campi Flegrei Caldera. Earth Planet. Sci. Lett. 414, 58–67.
Cook, A.C., Hainsworth, L.J., Sorey, M.L., Evans, W.C., 2001. Radiocarbon studies of plant leaves and tree rings from Mammoth Mountain, CA: a long-term record of magmatic CO_2 release. Chem. Geol. 177, 117–131.
Dawson, P.B., Evans, J.R., Iyer, H.M., 1990. Teleseismic tomography of the compressional wave velocity structure beneath the Long Valley region, California. J. Geophys. Res. 95, 11,021–11,050.
Dawson, P., Chouet, B., Pitt, A., 2016. Tomographic image of a seismically active volcano: Mammoth Mountain, California. J. Geophys. Res. 121:114–133. http://dx.doi.org/10.1002/2015JB012537.
Elbring, G.J., Rundle, J.B., 1986. Analysis of borehole seismograms from Long Valley, California: Implications for caldera structure. J. Geophys. Res. 91 (B12), 12,651–12,660.
Evans, B.W., Hildreth, W., Bachmann, O., Scaillet, B., 2016. In defense of magnetite-ilmenite thermometry in the Bishop Tuff and its implications for gradients in silicic magma reservoirs. Am. Mineral. 101, 469–482.
Farrar, C.D., Sorey, M.L., Evans, W.C., Howle, J.F., Kerr, B.D., Kennedy, B.M., King, C.-Y., Southon, J.R., 1995. Forest-killing diffuse CO_2 emission at Mammoth Mountain as a sign of magmatic unrest. Nature 376, 675–678.
Farrar, C.D., Sorey, M.L., Roeloffs, E., Galloway, D.L., Howle, J.F., Jacobson, R., 2003. Inferences on the hydrothermal system beneath the resurgent dome in Long Valley caldera, east-central California, USA, from recent pumping tests and geochemical sampling. J. Volcanol. Geotherm. Res. 127, 305–328.
Fialko, Y., Simons, M., Khazan, Y., 2001. Finite source modelling of magmatic unrest in Socorro, New Mexico, and Long Valley, California. Geophys. J. Int. 146, 191–200.
Fischer, M., Röller, K., Küster, M., Stöckhert, B., McConnell, V.S., 2003. Open fissure mineralization at 2600 m depth in Long Valley Exploratory Well (California)—insight into the history of the hydrothermal system. J. Volcanol. Geotherm. Res. 127, 347–363.
Foulger, G.R., Julian, B.R., Pitt, A.M., Hill, D.P., Malin, P.E., Shalev, E., 2003. Three-dimensional crustal structure of Long Valley caldera, California, and evidence for the migration of CO_2 under Mammoth Mountain. J. Geophys. Res. 108 (B3):2147. http://dx.doi.org/10.1029/2000JB000041 (15 p).
Fournier, R.O., 1999. Hydrothermal processes related to movement of fluid from plastic into brittle rock in the magmatic-epithermal environment. Econ. Geol. 94, 1193–1212.
Gerlach, T.M., Doukas, M.P., McGee, K.A., Kessler, R., 1999. Airborne detection of diffuse carbon dioxide emissions at Mammoth Mountain, California. Geophys. Res. Lett. 26 (24), 3661–3664.
Greene, D.C., Stevens, C.H., 2002. Geologic map of Paleozoic rocks in the Mount Morrison Pendant, eastern Sierra Nevada, California. California Division of Mines and Geology Map Sheet. 53 (scale 1:24,000).
Hauksson, E., 1988. Absence of evidence for a shallow magma chamber beneath Long Valley caldera, California, in downhole and surface seismograms. J. Geophys. Res. 93, 13,251–13,264.
Heumann, A., 1999. Timescales of Processes Within Silicic Magma Chambers. (PhD thesis). Vrije Universiteit, Amsterdam (200 p).
Heumann, A., Davies, G.R., Elliott, T., 2002. Crystallization history of rhyolites at Long Valley, California, inferred from combined U-series and Rb-Sr isotope systematics. Geochim. Cosmochim. Acta 66 (10), 1821–1837.
Hildreth, W., 2004. Volcanological perspectives on Long Valley, Mammoth Mountain, and Mono Craters: several contiguous but discrete systems. J. Volcanol. Geotherm. Res. 136, 169–198.
Hildreth, W., 2017. Concealed ring-fault zone of Long Valley caldera: International Association of Volcanology and Chemistry of Earth's Interior, excursion guides, Portland (Oregon) General Assembly, August 2017. US Geol. Surv. Sci. Investig. Rep. 2016–5022 (14 p).
Hildreth, W., Fierstein, J., 2016a. Eruptive history of Mammoth Mountain and its mafic periphery. U.S. Geological Survey Professional Paper. 1812 (128 p., 1:24,000 geologic map).
Hildreth, W., Fierstein, J., 2016b. Long Valley caldera lake and reincision of Owens River Gorge. U.S. Geological Survey Scientific Investigations Report. 5120 (accepted, in press).
Hildreth, W., Wilson, C.J.N., 2007. Compositional zoning of the Bishop Tuff. J. Petrol. 48, 951–999.
Hildreth, W., Fierstein, J., Champion, D., Calvert, A., 2014. Mammoth Mountain and its mafic periphery—a late Quaternary volcanic field in eastern California. Geosphere 10 (6), 1315–1365.
Hildreth, W., Fierstein, J., Calvert, A., 2017. Early postcaldera rhyolite and structural resurgence at Long Valley caldera, California. J. Volcanol. Geotherm. Res. 335, 1–34.
Hill, D.P., 1976. Structure of Long Valley caldera, California, from a seismic refraction experiment. J. Geophys. Res. 81, 745–753.
Hill, D.P., 1992. Temperatures at the base of the seismogenic crust beneath Long Valley Caldera, California, and the Phlegrean Fields Caldera, Italy. In: Gasparini, P., Scarpa, R., Aki, K. (Eds.), Volcanic Seismology: IAVCEI Proceedings in Volcanology. vol. 3. Springer Verlag, Berlin, pp. 432–461.
Hill, D.P., 2006. Unrest in Long Valley caldera, California, 1978-2004. In: De Natale, G., et al. (Eds.), Mechanisms of Activity and Unrest at Large Calderas. 269. Geological Society of London Special Publication, pp. 1–24.
Hill, D.P., Montgomery-Brown, E., 2015. Long Valley caldera and the UCERF depiction of Sierra Nevada range-front faults. Bull. Seismol. Soc. Am. 105 (6), 3189–3195.
Hill, D.P., Dzurisin, D., Ellsworth, W.L., Endo, E.T., Galloway, D.L., Gerlach, T.M., Johnston, M.J.S., Langbein, J., McGee, K.A., Miller, C.D., Oppenheimer, D., Sorey, M.L., 2002. Response plan for volcano hazards in the Long Valley caldera and Mono Craters region, California. U.S. Geol. Surv. Bull. 2185 (57 p).
Hill, D.P., Langbein, J.O., Prejean, S., 2003. Relations between seismicity and deformation during unrest in Long Valley caldera, California, from 1995 through 1999. J. Volcanol. Geotherm. Res. 127, 175–193.
Hill, D.P., Mangan, M.T., McNutt, S.R., 2016. Volcanic unrest and hazard communication in Long Valley volcanic region, California. In: Fearnley, C., Bird, D., Jolly, G., Haynes, K., McGuire, B. (Eds.), Observing the Volcano World. Springer (in press).

Hurwitz, S., Christiansen, L.B., Hsieh, P.A., 2007. Hydrothermal fluid flow and deformation in large calderas: Inferences from numerical simulations. J. Geophys. Res. 112, B02206. http://dx.doi.org/10.1029/2006JB004689.
Hurwitz, S., Farrar, C.D., Williams, C.F., 2010. The thermal regime in the resurgent dome of Long Valley caldera, California: Inferences from precision temperature logs in deep wells. J. Volcanol. Geotherm. Res. 198, 233–240.
Hutnak, M., Hurwitz, S., Ingebritsen, S.E., Hsieh, P.E., 2009. Numerical models of caldera formation: Effects of multiphase and multicomponent hydrothermal fluid flow. J. Geophys. Res. 114, B04411. http://dx.doi.org/10.1029/2008JB006151.
Kelleher, P.C., Cameron, K.L., 1990. The geochemistry of the Mono Craters–Mono Lake Islands volcanic complex, eastern California. J. Geophys. Res. 95, 17643–17659.
Kissling, E., 1988. Geotomography with local earthquake data. Rev. Geophys. 26 (4), 659–698.
Langbein, J., 1989. Deformation of the Long Valley Caldera, Eastern California from mid-1983 to mid-1988: measurements using a two-color geodimeter. J. Geophys. Res. 94 (B4), 3833–3849.
Langbein, J.O., 2003. Deformation of the Long Valley caldera, California: inferences from measurements from 1998 to 2001. J. Volcanol. Geotherm. Res. 127, 247–267.
Langbein, J., Linker, M., Tupper, D., 1987. Analysis of two-color geodimeter measurements of deformation within the Long Valley caldera: June 1983 to October 1985. J. Geophys. Res. 92 (B9), 9423–9442.
Langbein, J., Hill, D.P., Parker, T.N., Wilkinson, S.K., 1993. An episode of reinflation of the Long Valley Caldera, eastern California: 1989–1991. J. Geophys. Res. 98 (B9), 15,851–15,870.
Langbein, J., Dzurisin, D., Marshall, G., Stein, R., Rundle, J., 1995. Shallow and peripheral volcanic sources of inflation revealed by modelling two-color geodimeter and leveling data from Long Valley caldera, California, 1988–1992. J. Geophys. Res. 100 (B7), 12,487–12,495.
LeBas, M.J., LeMaitre, R.W., Streckeisen, A., Zanettin, B., 1986. A chemical classification of volcanic rocks based on the total alkali–silica diagram. J. Petrol. 27, 745–750.
Lejeune, A.-M., Richet, P., 1995. Rheology of crystal-bearing silicate melts: an experimental study at high viscosities. J. Geophys. Res. 100 (B3), 4215–4229.
Lewicki, J.L., Hilley, G.E., Shelly, D.R., King, J.C., McGeehin, J.P., Mangan, M., Evans, W.C., 2014. Crustal migration of CO_2-rich magmatic fluids recorded by tree-ring radiocarbon and seismicity at Mammoth Mountain, CA, USA. Earth Planet. Sci. Lett. 390, 52–58.
Lin, G., 2015. Seismic velocity structure and earthquake relocation for the magmatic system beneath Long Valley Caldera, eastern California. J. Volcanol. Geotherm. Res. 296, 19–30.
Lucic, G., Stix, J., Wing, B., 2015. Structural controls on the emission of magmatic carbon dioxide gas, Long Valley caldera, USA. J. Geophys. Res. Solid Earth 120:2262–2278. http://dx.doi.org/10.1002/2014JB011760.
Luetgert, J.H., Mooney, W.D., 1985. Crustal refraction profile of the Long Valley caldera, California, from the January 1983 Mammoth Lakes earthquake swarm. Bull. Seismol. Soc. Am. 75 (1), 211–221.
Marsh, B.D., 1981. On the crystallinity, probability of occurrence, and rheology of lava and magma. Contrib. Mineral. Petrol. 78, 85–98.
McConnell, V.S., Shearer, C.K., Eichelberger, J.C., Keskinen, M.J., Layer, P.W., Papike, J.J., 1995. Rhyolite intrusions in the intracaldera Bishop Tuff, Long Valley caldera, California. J. Volcanol. Geotherm. Res. 67, 41–60.
McConnell, V.S., Valley, J.W., Eichelberger, J.C., 1997. Oxygen isotope compositions of intracaldera rocks: hydrothermal history of the Long Valley caldera, California. J. Volcanol. Geotherm. Res. 76, 83–109.
Metz, J.M., Mahood, G.A., 1985. Precursors to the Bishop Tuff eruption: Glass Mountain, Long Valley, California. J. Geophys. Res. 90, 11,121–11,126.
Metz, J.M., Mahood, G.A., 1991. Development of the Long Valley, California, magma chamber recorded in precaldera rhyolite lavas of Glass Mountain. Contrib. Mineral. Petrol. 106, 379–397.
Montgomery-Brown, E.K., Wicks, C.W., Cervelli, P.F., Langbein, J.O., Svarc, J.L., Shelly, D.R., Hill, D.P., Lisowski, M., 2015. Renewed inflation of Long Valley caldera, California (2011 to 2014). Geophys. Res. Lett.:42 http://dx.doi.org/10.1002/2015GL064338.
Newman, A.V., Dixon, T.H., Gourmelen, N., 2006. A four-dimensional viscoelastic deformation model for Long Valley Caldera, California, between 1995 and 2000. J. Volcanol. Geotherm. Res. 150, 244–269.
Peacock, J.R., Mangan, M.T., McPhee, D., Wannamaker, P.E., 2016. Three-dimensional electrical resistivity model of the hydrothermal system in Long Valley Caldera, California, from magnetotellurics. Geophys. Res. Lett. 43, 7953–7962.
Phillips, F.M., Majkowski, L., 2011. The role of low-angle normal faulting in active tectonics of the northern Owens Valley, California. Lithosphere 3 (1), 22–36.
Ponko, S.C., Sanders, C.O., 1994. Inversion for P and S wave attenuation structure, Long Valley caldera, California. J. Geophys. Res. 99, 2619–2635.
Prejean, S., Ellsworth, W., Zoback, M., Waldhauser, F., 2002. Fault structure and kinematics of the Long Valley caldera region, California, revealed by high-accuracy earthquake hypocenters and focal mechanism stress inversions. J. Geophys. Res. 107 (B12): 2355. http://dx.doi.org/10.1029/2001JB001168.
Pribnow, D.F.C., Schütze, C., Hurter, S.J., Flechsig, C., Sass, J.H., 2003. Fluid flow in the resurgent dome of Long Valley caldera: implications from thermal data and deep electrical sounding. J. Volcanol. Geotherm. Res. 127, 329–345.
Reid, M.R., Coath, C.D., Harrison, T.M., McKeegan, K.D., 1997. Prolonged residence times for the youngest rhyolites associated with Long Valley caldera; ^{230}Th-^{238}U ion microprobe dating of young zircons. Earth Planet. Sci. Lett. 150, 27–39.
Rinehart, C.D., Ross, D.C., 1964. Geology and mineral deposits of the Mount Morrison Quadrangle, Sierra Nevada, California. US Geol. Surv. Prof. Pap. 385 (106 p).
Roberge, J., Wallace, P.J., Kent, A.J.R., 2013. Magmatic processes in the Bishop Tuff rhyolitic magma based on trace elements in melt inclusions and pumice matrix glass. Contrib. Mineral. Petrol. 165, 237–257.
Romero Jr., A.E., McEvilly, T.V., Majer, E.L., 1993. Velocity structure of the Long Valley caldera from the inversion of local earthquake P and S travel times. J. Geophys. Res. 98, 19,869–19,879.
Sampson, D.E., Cameron, K.L., 1987. The geochemistry of the Inyo volcanic chain: Multiple magma systems in the Long Valley region, eastern California. J. Geophys. Res. 92 (B10), 10,403–10,421.
Sanders, C.O., 1984. Location and configuration of magma bodies beneath Long Valley, California, determined from anomalous earthquake signals. J. Geophys. Res. 89, 8287–8302.
Sanders, C.O., 1993. Reanalysis of S-to-P amplitude ratios for gross attenuation structure, Long Valley caldera, California. J. Geophys. Res. 98, 22,069–22,079.
Sanders, C.O., Ponko, S.C., Nixon, L.D., Schwartz, E.A., 1995. Seismological evidence for magmatic and hydrothermal structure in Long Valley caldera from local earthquake attenuation and velocity tomography. J. Geophys. Res. 100 (B5), 8311–8326.
Savage, J.C., Lisowski, M., 1984. Deformation in the White Mountain Seismic Gap, California-Nevada, 1972–1982. J. Geophys. Res. 89 (B9), 7671–7687.
Savage, J.C., Cockerham, R.S., Estrem, J.E., Moore, L.R., 1987. Deformation near the Long Valley Caldera, eastern California, 1982–1986. J. Geophys. Res. 92 (B3), 2721–2746.
Scaillet, B., Hildreth, W., 2001. In: Knesel, K., Bergantz, G.B., Davidson, J. (Eds.), Experimental constraints on the origin and evolution of the Bishop Tuff, 5 p. Penrose Conference, Mammoth Lakes, California: Longevity and Dynamics of Rhyolitic Magma Systems. Geological Society of America (230 p).
Seccia, D., Chiarabba, C., DeGori, P., Bianchi, I., Hill, D.P., 2011. Evidence for the contemporary magmatic system beneath Long Valley Caldera from local earthquake tomography and receiver function analysis. J. Geophys. Res. 116, B12314. http://dx.doi.org/10.1029/2011JB008471.
Shelly, D.R., Hill, D.P., 2011. Migrating swarms of brittle-failure earthquakes in the lower crust beneath Mammoth Mountain, California. Geophys. Res. Lett. 38, L20307. http://dx.doi.org/10.1029/2011GL049336.
Shelly, D.R., Ellsworth, W.L., Hill, D.P., 2016. Fluid-faulting evolution in high definition: Connecting fault structure and frequency-magnitude variations during the 2014 Long Valley Caldera, California, earthquake swarm. J. Geophys. Res. Solid Earth 121. http://dx.doi.org/10.1002/2015JB012719.
Sisson, T.W., Bacon, C.R., 1999. Gas-driven filter pressing in magmas. Geology 27, 613–616.
Sorey, M.L., Suemnicht, G.A., Sturchio, N.C., Nordquist, G.A., 1991. New evidence on the hydrothermal system in Long Valley caldera, California, from wells, fluid sampling, electrical geophysics, and age determinations of hot-spring deposits. J. Volcanol. Geotherm. Res. 48, 229–263.
Sorey, M.L., Kennedy, B.M., Evans, W.C., Farrar, C.D., Suemnicht, G.A., 1993. Helium isotope and gas discharge variations associated with crustal unrest in Long Valley Caldera, California, 1989–1992. J. Geophys. Res. 98 (B9), 15,871–15,889.
Steck, L.K., Prothero Jr., W.A., 1994. Crustal structure beneath Long Valley caldera from modeling of teleseismic P-wave polarizations and S-P converted phases. J. Geophys. Res. 99, 6881–6898.
Steeples, D.W., Iyer, H.M., 1976. Low velocity zone under Long Valley as determined from teleseismic events. J. Geophys. Res. 81, 849–860.
Suemnicht, G.A., 1987. Results of deep drilling in the western moat of Long Valley, California. Eos 68 (40), 785–798.
Suemnicht, G.A., Sorey, M.L., Moore, J.N., Sullivan, R., 2006. The shallow hydrothermal system of Long Valley caldera, California. Geotherm. Resour. Counc. Trans. 30, 465–469.
Suemnicht, G.A., Kennedy, B.M., Evans, W.C., 2015. Helium isotope systematics of Long Valley Caldera, California. Proceedings, World Geothermal Congress 2015, Melbourne, Australia, pp. 1–6.
Thatcher, W., Massonnet, D., 1997. Crustal deformation at Long Valley Caldera, eastern California, 1992–1996 inferred from satellite radar interferometry. Geophys. Res. Lett. 24 (20), 2519–2522.
Tiampo, K.F., Rundle, J.B., Fernandez, J., Langbein, J.O., 2000. Spherical and ellipsoidal volcanic sources at Long Valley caldera, California, using a genetic algorithm inversion technique. J. Volcanol. Geotherm. Res. 102, 189–206.
Tizzani, P., Battaglia, M., Zeni, G., Atzori, S., Berardino, P., Lanari, R., 2009. Uplift and magma intrusion at Long Valley caldera from InSAR and gravity measurements. Geology 37, 63–66.
Tuttle, O.F., Bowen, N.L., 1958. Origin of granite in the light of experimental studies in the system $NaAlSi_3O_8$–$KAlSi_3O_8$–SiO_2–H_2O. Geol. Soc. Am. Memoir 74 (153 p).
Vanorio, T., Kanitpanyacharoen, W., 2015. Rock physics of fibrous rocks akin to Roman concrete explains uplifts at Campi Flegrei Caldera. Science 349 (6248), 617–621.
Varga, R.J., Bailey, R.A., Suemnicht, G.A., 1990. Evidence for 600-year-old basalt and magma mixing at Inyo Craters volcanic chain, Long Valley caldera, California. J. Geophys. Res. 95 (B13), 21,441–21,450.
Waldhauser, F., 2009. Near-real-time double-difference event location using long-term seismic archives, with application to Northern California. Bull. Seismol. Soc. Am. 99: 2736–2748. http://ddrt.ldeo.columbia.edu/DDRT/index.html.
Wallace, P.J., Anderson Jr., A.T., Davis, A.M., 1999. Gradients in H_2O, CO_2, and exsolved gas in a large-volume silicic magma system: Interpreting the record preserved in melt inclusions from the Bishop Tuff. J. Geophys. Res. 104, 20,097–20,122.
Waters, L.E., Lange, R.A., 2014. Evidence for an abrupt transition in the mantle-derived source to the Long Valley Caldera rhyolites after the climactic eruption: from subduction-modified lithosphere to asthenosphere. American Geophysical Union, Fall Meeting, Abstract. V33A–4829.
Weiland, C.M., Steck, L.K., Dawson, P.B., Korneev, V.A., 1995. Nonlinear teleseismic tomography at Long Valley caldera, using three-dimensional minimum travel time ray tracing. J. Geophys. Res. 100 (B10), 20,379–20,390.
Werner, C., Bergfeld, D., Farrar, C.D., Doukas, M.P., Kelly, P.J., Kern, C., 2014. Decadal-scale variability of diffuse CO_2 emissions and seismicity revealed from long-term monitoring (1995–2013) at Mammoth Mountain, California, USA. J. Volcanol. Geotherm. Res. 289, 51–63.